©2021

NAMARIQ AL’SAADI

ALL RIGHTS RESERVED

MAGNESIUM MODULATES CELLULAR ROS LEVELS TO CONTROL CYTOSKELETAL REMODELING

by

NAMARIQ AL-SAADI

A dissertation submitted to the

School of Graduate Studies

Rutgers, The State University of New Jersey

In partial fulfillment of the requirements

For the degree of

Doctor of Philosophy

Graduate Program in Cellular and Molecular Pharmacology

Written under the direction of

Loren W. Runnels, Ph.D.

And approved by

_____

_____

_____

_____

_____

New Brunswick, New Jersey

June 2021

ABSTRACT OF THE DISSERTATION

MAGNESIUM MODULATES CELLULAR ROS LEVELS TO CONTROL CYTOSKELETAL REMODELING

By NAMARIQ AL-SAADI

Dissertation Director:

Loren W. Runnels, Ph.D.

Evidence for putative second messenger functions for Mg^{2+} has quietly accumulated for decades. Bound to DNA, RNA, and ATP and functioning as a cofactor for over 600 different enzymes, an enduring mystery is how signal discrimination is achieved when Mg^{2+} is the second most abundant cation in the cell. We previously showed that depletion of the TRPM7 ion channel from fibroblasts reduces intracellular Mg^{2+}, interfering with the actin cytoskeleton's remodeling during polarized cell movements. Defects in cell spreading and formation of actin stress fibers caused by loss of the channel can be rescued by overexpression of the magnesium transporter SLC41A2. Here we report that Mg^{2+} controls remodeling of the actin cytoskeleton independent of microtubules by regulating the concentration of reactive oxygen species (ROS) in cells. A lowering of ROS levels accompanies a reduction in cellular Mg^{2+} caused by depletion of the

TRPM7 ion channel. Raising ROS levels independent of Mg^{2+} rescued defects in cell spreading caused by depletion of the channel. To test whether Mg^{2+} acts independent of TRPM7 to regulate the actin cytoskeleton we overexpressed the Mg^{2+} exporter CNNM2 in fibroblasts to lower intracellular Mg^{2+}, which we found also lowered ROS levels and produced similar defects in the cellular distribution of actin but not microtubules similar to that observed for cellular depletion of TRPM7. Reducing ROS levels independent of changes in cellular Mg^{2+} by overexpression of the ROS scavenger catalase produced similar changes in the cytoskeleton and cell morphology. Mg^{2+}-dependent changes in cellular ROS results in the oxidation of numerous proteins, including those involved in cytoskeletal remodeling. We conclude that signal transduction via changes in intracellular Mg^{2+} signals occur by Mg^{2+}-dependent changes in cellular ROS levels.

ACKNOWLEDGMENTS

Many people have supported me on my journey to earning my Ph.D. by giving me confidence, support, and encouragement. I am deeply appreciative to my supervisor, Dr. Loren Runnels, for teaching me how to be successful and for motivating me to achieve my goals without any pressure or cause for depression. He helped me to overcome my language obstacles. He was my pacemaker, helping me find my destiny. I always felt his support. I do not have enough words to express my gratitude for him, but as long as I live, I will spread his message of optimism and teamwork. Thank you for everything. I was greatly honored to be your student.

I am also sincerely thankful to my other thesis committee members, Dr. Nancy Walworth, Dr. Beatrice Haimovich, and Dr. Huizhou Fan for their suggestions and feedback. I would like to thank my lab members, especially Na Cai, who graduated two years before me. Whenever I had a problem or a question, I could turn to her and know she could help me. Na was a very helpful and hardworking student from who I learned a lot. I also want to thank my current lab members, including postdoctoral fellow Dr. Zhiyong Bai. I am grateful to him for giving me the chance to work with him on his project, which gave me added experience and training. I will never forget the words he always told me, “Do not worry and I trust you.” Zhiyong's words of encouragement made me feel more confident in my abilities. Thank you, Zhiyong! I was also very happy to share my training experience with Dr. Liping Lou. She made lab members feel like we were part of a team. Liping

made the culture of the lab joyful, as we all strived to win the "game" by getting the "ball into the goal." I am also thankful to Sandra Tetteh who was always helpful and kind with her advice, never hesitating to share her experience. I also felt like I had a sister in the lab, Thank you Sandra! I also am thankful for the company of other members of the lab, including Thushara Nethramangalath and Dr. Jeremy Willekens, who were essential members of the lab team.

I also want to extend my gratitude to those who helped me when I first joined the lab; they helped me take my first steps as a scientist. My thanks to former lab member Dr. Yuko Komiya for sharing her experience and Jeffrey Overton, who I only knew for a short time, from whom I learned a lot.

My sincere appreciation to all the members of the Pharmacology department who made it feel like a warm home. Thank you, Lucyna for all work you have done for us, and for your smile, which always communicated hope and life.

I can say there is no life without friends. Thank you to all my dear friends, who shared my journey with big smiles. We carried our obstacles together. I would like to thank my friends, Ansab Krkoosh, Afrah Al-Obaidi, Rawasi Al-Asadi, Najia Al-Baiti, Nuble Al-Baiti, and Rowida Mohammed.

Also, I wanted to acknowledge the Ministry of Higher Education and Scientific Research in Iraq for their financial support during my Ph.D. training.

My warm regard and gratitude to the warm sun that is my parents. Together they are the light of my life, who shined with love and support and helped me to attain happiness and achieve goals. Thank you to my mother-in-law and father-in-law for praying for my family and your kind wishes for us.

Thank you to all my sisters and brothers!! You are all with me all the time.

Without his first words of encouragement, I would not have had this amazing journey. He told me to not look backward, and we will go forward together. I am grateful to my husband for how far we have come and how he always supports me in our journey. Our journey together has given me the love, life, strength, and hope of our sweet children, Alirada, Fatimah, and Noor Fatimah.

Dedication

To my country……Iraq

and

To everyone who taught me a letter

TABLE OF CONTENTS

LIST OF FIGURES

INTRODUCTION

1. TRPM7

TRPM7 is a unique fusion of ion channel with a serine/threonine kinase domain attached to its COOH-terminus[1, 2]. The bifunctional channel is expressed in nearly all cells and is highly permeable to divalent cations, including Mg^{2+}, Ca^{2+}, and Zn^{2+}[3]. Several studies have shown a role for TRPM7 in controlling cytoskeleton remodeling and cell migration through its ability to affect both cellular Ca^{2+} and Mg^{2+} homeostasis[4-6]. Knockout approaches in mice have revealed an essential role for the channel-kinase in early embryonic development and organogenesis[7, 8].

Although permeable to Ca^{2+} and Zn^{2+} (Fig 1), TRPM7 is considered to be one of the main avenues for Mg^{2+} entry into the cells, among other Mg^{2+} transporters such as SLC41A1/2, MagT1, Mrs2, and TRPM6 (6). Depletion of the channel at cellular level by RNA interference or by targeted antisense morpholinos leads to defects in cell proliferation, cell migration, and cytoskeletal organization as shown in cell culture, stem cells, and *Xenopus laevis* embryos [9-11]. Interestingly, these defects can be rescued by Mg^{2+} supplementation of the growth media or by overexpression of the Mg^{2+} transporter SLC41A2 or MagT1.

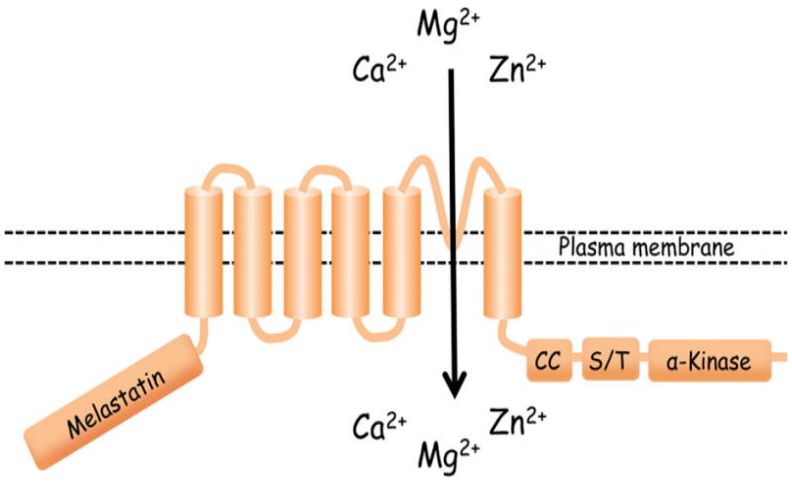

Figure 1 Schematic model of the membrane topology of TRPM7.

TRPM7 has 6 transmembrane domains and a pore-loop that is localized between fifth and sixth transmembrane domains[12].

2. Magnesium

With an intracellular concentration ranging from 14 to 20 mM, magnesium (Mg^{2+}) is the second most abundant intracellular cation[13]. Unlike Ca^{2+}, whose cytosolic concentration can vary 10-100-fold, the free concentration of Mg^{2+} is comparably steady, hovering between 0.4 – 1 mM in concentration[13]. This has led some to question whether Mg^{2+} can function as a second messenger like Ca^{2+}[14]. Nevertheless Mg^{2+} is critical to the function of cells, influencing a wide range biological functions, from cell proliferation to protein synthesis [15]. Indeed, it has been estimated that at least 600 enzymatic reactions are directly or indirectly regulated by Mg^{2+} [13]. And Mg^{2+} itself binds as a co-factor to over 200 other proteins, including some that compose the cytoskeleton [13]

3. Magnesium and the Cytoskeleton

The earliest report of an effect of magnesium (Mg^{2+}) on the cytoskeleton came from the work of Prescott and colleagues [16]. These researchers observed that microinjection of 10 mM $MgSO_4$, which raised the concentration of intracellular free Mg^{2+} to 1 mM, destabilized the cytoskeleton by altering microtubules [16]. In a more recent study, investigators compared the cytoskeleton of endothelial cells maintained in normal Mg^{2+} (2 mM) versus in low Mg^{2+} (0.1 mM) [6]. The authors reported that compared to low Mg^{2+} conditions, Mg^{2+} treatment of cells induced significant cytoskeletal reorganization, with more F-actin and microtubules present inside the cells bathed in high Mg^{2+}, compared to the localization of these cytoskeletal elements to the cell periphery under low Mg^{2+} conditions [6].

It wasn't until specific magnesium transporters and ion channels were identified, that it was understood that directly manipulating intracellular magnesium levels can produce profound effects on the cytoskeleton. Overexpression of TRPM7 in HEK-293 cells was first observed to cause cell rounding and loss of adhesion [2]. Later work showed TRPM7 activates calpain to produce cell rounding and loss of cell adhesion[17]. Overexpression of TRPM7 increases cellular Mg^{2+} as well as Ca^{2+} to stimulate the activity of the m-calpain isoform [18]. Conversely, depletion of the channel in HEK-293 cells increased cell spreading [17]. Later work has shown that knockdown of TRPM7 affects the cytoskeleton and the migratory properties of diverse cell types, including many types of cancer cells [17, 19-25]. Conversely, activation of TRPM7 with the molecule naltriben stimulates cell migration[26]. In human microvascular endothelial cells (HMEC), in particular, it was

reported silencing of TRPM7 protein expressions mimics the effect that exposing cells to low extracellular Mg^{2+} has on the cell migration [20]. When TRPM7 was knocked down in Swiss 3T3 cells, the cell shape was transformed from a spread to spindle-like morphology [25]. The change in cell shape could be rescued by re-expressing TRPM7 but also by overexpressing the magnesium transporter SLC41A2[25]. TRPM7-knockdown fibroblasts also had diminished stress fiber formation and were unable to execute changes in cell polarity and directional cell migration [25]. In endothelial cells, depletion of TRPM7 and MagT1 by siRNA was also reported to affect cytoskeletal reorganization in an Mg^{2+}-dependent manner [6]. Loss of TRPM7 and/or MagT1 in these cells also affected intracellular junctions by affecting the protein expression of ZO-1, Cadherin, and Occludin [6].

4. Evidence that Magnesium Regulates Cell Migration and the Cytoskeleton In Vivo.

Only a handful of studies have demonstrated a role for Mg^{2+} *in vivo*, however, the evidence has been compelling. Platelets are derived from megakaryocytes in the bone marrow through a process which is driven by the cytoskeleton. TRPM7 was identified as a key Mg^{2+} channel in murine platelets [27]. Human patients containing megakaryocytes with mutations in TRPM7 also had a defect in platelet formation and megakaryocytes cytoskeleton[27]. To better understand the origin of the human defect, TRPM7 was conditionally knocked-out in murine megakaryocytes, which was found to cause cytoskeletal alterations that impaired proplatelet formation[27]. In particular, the content and organization of

microtubules in megakaryocytes was disrupted. In addition, the localization and protein stability of myosin IIA was altered. The alterations to the megakaryocyte's cytoskeleton could be rescued by Mg^{2+} supplementation but not by Ca^{2+} supplementation[27]. Interestingly, application of the myosin II inhibitor blebbistatin was also able to rescue the defect in megakaryocytes caused by knockout of TRPM7 [27]. This data suggests that Mg^{2+} exerts its affect, at least in part, by affecting the activity of non-muscle myosin IIA, and perhaps microtubules as well.

A role for Mg^{2+} and cell migration was also uncovered in early embryonic development. When globally deleted from mice, the TRPM7 ion channels causes early embryonic death at embryonic day 7.5 [7]. To investigate the mechanism by which TRPM7 regulates embryogenesis, investigators studied how depletion of TRPM7 in *Xenopus laevis* embryos using an antisense TRPM7 morpholino affects development. Loss of TRPM7 produced a gastrulation phenotype, in which morphogenesis of the embryo failed due to a disruption in convergent extension cell movements [9]. Surprisingly, the gastrulation defects caused by loss of TRPM7 protein expression could be rescued by supplementing the buffer containing the embryos with high Mg^{2+} or by co-expression of the Mg^{2+} transporter SLC41A2 with the TRPM7 morpholino. In a more recent study, a role for TRPM6 in neural tube closure was revealed in mice [28]. TRPM6 is the ion channel whose gene is mutated in familial hypomagnesemia with secondary hypocalcemia (HSH) disease [29, 30]. Studies in *Xenopus laevis* showed that TRPM6 regulates radial intercalation cell movements in the lateral mesoderm during neural tube closure [31]. Importantly, the defect caused by loss of TRPM6 could be suppressed by expression of the Mg^{2+}

transporter SLC41A2. These experiments demonstrated that the *Xenopus laevis* organism regulates intracellular Mg^{2+} concentrations to regulate cell movements during early embryonic development. The mechanism(s) by which Mg^{2+} exerts its profound effects on the cytoskeleton remain poorly understood.

5. ROS and the Cytoskeleton.

Interestingly, lowering Mg^{2+} in response to knockdown of TRPM7 is Swiss 3T3 fibroblasts was reported to decrease intracellular reactive oxygen species (ROS) levels [32]. Conversely, overexpression of TRPM7 has also been shown to raise intracellular Mg^{2+} and cellular ROS levels [32]. Whether there is a connection between Mg^{2+}, ROS, and the cytoskeleton has never been investigated.

ROS is generally defined as reactive molecules containing oxygen. Some common ROS produced in the cell include superoxide ($O2^{\cdot -}$), hydrogen peroxide (H_2O_2), peroxynitrite ($OONO^-$), and the hydroxyl radical ($HO^{\cdot}$), which are all produced in biological systems. ROS was originally viewed as a toxic byproduct of the cell, which can cause cell damage and even cell death [33]. Now it is appreciated that ROS levels are stringently regulated by the activity of many intracellular enzymes and can function as a signaling molecule to regulate biological and physiological processes [34]. $OONO^-$ and $HO^{\cdot}$ are not considered as signaling molecules because of their high reactivity, irreversible modifications that contribute to oxidative stress and pathologic damage to tissues. There are at least three main sources of ROS in the cell that can function in cell signaling [35]. The first results in the generation of $O_2^{\cdot -}$ from the activity of the electron transport chain in

mitochondria as a byproduct of respiration[36]. A second source is from lipoxygenases, which catalyze the oxidation of polyunsaturated fatty acids[35]. And the third source of ROS naturally produced in cells is from NADPH oxidase, which produces $O_{2^{\cdot -}}$ and is one of the best understood enzymes in terms of ROS signaling [37]. NADPH oxidase enzymes make up a family of five isoforms [37]. Each isoform has additional subunits that control catalytic activity to generate $O_{2^{\cdot}}$. Later in this thesis we will be describing our use of NADPH oxidase 1 (NOX) and its regulators NOXO1 and NOXA1 as a tool to artificially raise cellular ROS levels. First, we will describe what is currently known about ROS and its control of the cytoskeleton.

It was through the study of ROS production by NADPH oxidase that it was discovered that ROS influences cell signaling [37]. It is now recognized that ROS can modulate the activities of numerous proteins involved in the control of the cytoskeleton (Figure 2). For example, it was found that intracellular ROS are generated after integrin engagement and that the production of ROS was necessary for integrin signaling during fibroblast adhesion and spreading [38]. One of the main targets of ROS signaling is tyrosine phosphatases, whose activities are dependent on the redox state of a low pKA active site cysteine [38]. The redox-sensitive phosphatases include LMW-PTP, Shp2, the tyrosine phosphatase PTP-PEST and PTP1B [35]. Inhibition of these phosphatases by oxidation prolongs the phosphorylation state of many phosphoproteins, include Cofilin, FAK, Src, PI3K, PKC and Rho GTPase, which themselves regulate the cytoskeleton [35]. And of course, components of the cytoskeleton are also targeted by oxidation, including actin, myosin II and tubulin [39, 40].

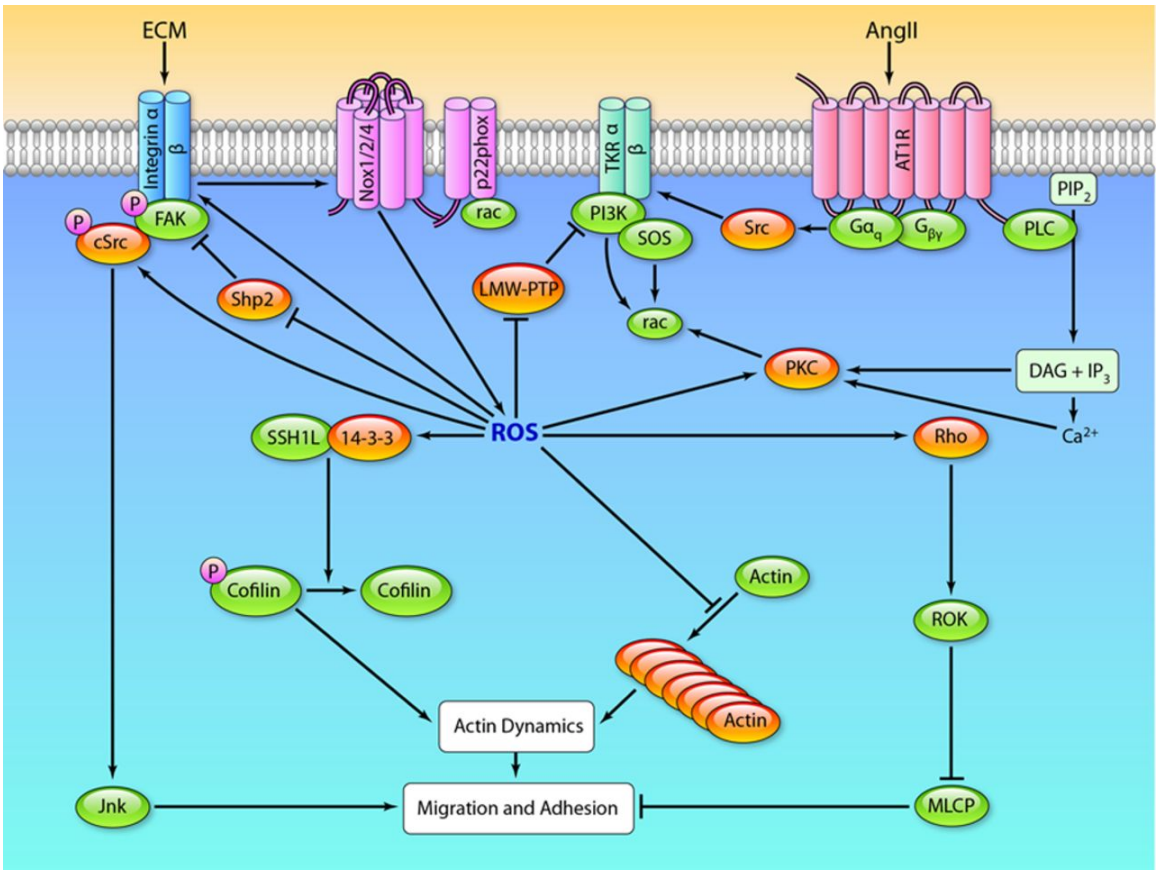

Figure 2 Redox signaling pathways in migration and adhesion (taken from (35)).

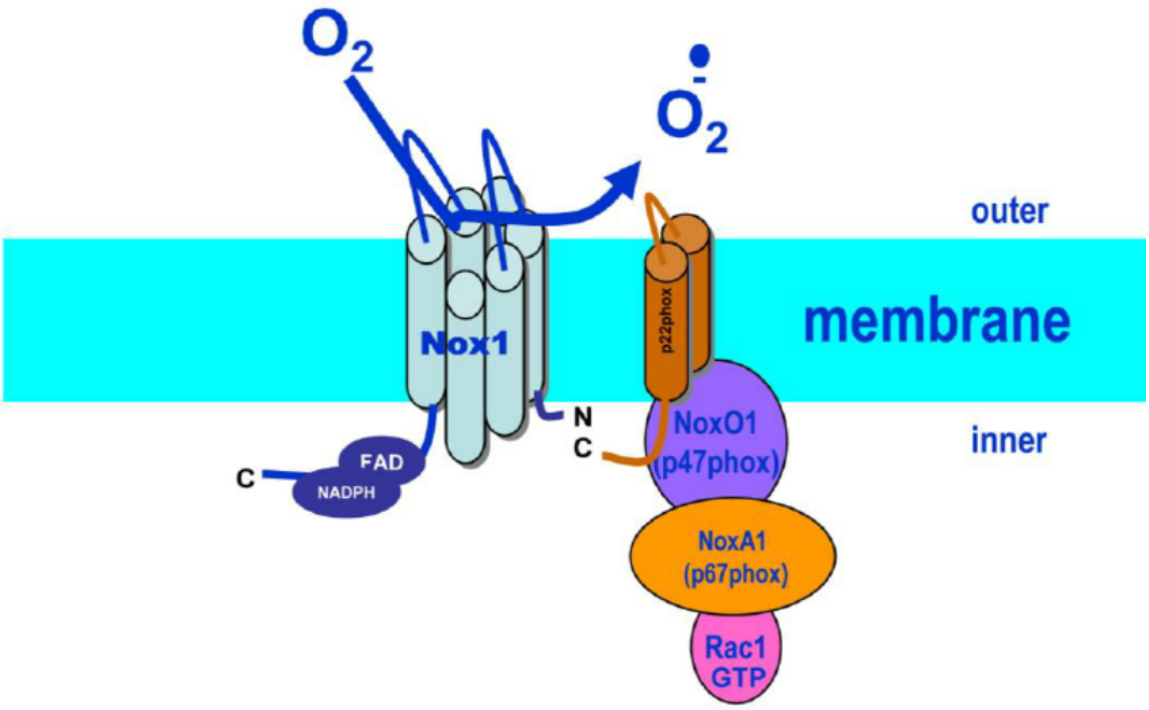

Figure 3 Nox1 and its regulatory subunits NoxO1, NoxA1, and Rac1 (adapted from (41)).

6. CNNM and ARL15 Proteins

Later in the Experimental Results, Section 3, we will describe how we employed the protein CNNM2 as a tool to lower intracellular Mg^{2+} in cells. A significant part of my time in the Runnels lab was also devoted to investigating the role of CNNMs and its binding protein ARL15 on TRPM7 channel function and regulation, which we describe in Experimental Results, Sections 4 and 5.

Members of the CNNM family have also shown to be involved in the control of Mg^{2+} homeostasis. CNNM1, CNNM2, CNNM3, and CNNM4 are

members of the CNNM family, which was previously known as ancient, conserved domain proteins (ACDP) in humans and mice[41, 42]. CNNMs are transmembrane proteins with a Bateman module made up of two cystathionine-beta-synthase (CBS) motifs[43, 44]. CNNMs' Bateman module binds to Mg^{2+}-ATP[45], which has been shown to cause significant structural changes in the Bateman module to regulate CNNM transport activity [46]. Members of the phosphatases regenerating liver (PRLs) family, which bind to the Bateman module, also regulate the activity of CNNMs[47, 48].

CNNMs, like TRPM7, have been related to illness. Mutations in human *Cnnm2* cause hypomagnesemia, owing to disruption of its function as either a basolateral Mg^{2+} extruder at the renal distal convoluted tubule [49], or as a Mg^{2+} homeostatic factor that controls Mg^{2+} transport at this site [50]. CNNM2 is also reported to be necessary for sperm motility[51], blood pressure control[52], and is highly expressed in the brain, with human mutations in *Cnnm2* linked to schizophrenia[53, 54], brain malformations, and epilepsy[49]. The function of CNNM2 is fiercely debated, with some researchers claiming CNNM2 operates as a simple transporter that extrudes Mg^{2+} ions from the basolateral side of polarized epithelial cells[44, 55]. While other researchers have concluded that CNNM2 does not actively participate in membrane transport, but rather serves as either intracellular Mg^{2+} sensors or as a Mg^{2+} homeostatic mediator of other unidentified transcellular transporters that control divalent cation influx and efflux processes[50]. In Section 4 of the Experimental Results, we present results

demonstrating that CNNM can regulate TRPM7-dependent divalent cation influx. In the absence of TRPM7, CNNM2 and CNNM4 appear to have robust Mg^{2+} efflux activity compared to CNNM1 and CNNM3, giving strong evidence that CNNMs mediate Mg^{2+} efflux independent of TRPM7[56]. In comparison to CNNM2 and CNNM4, CNNM3 has been found necessary for Mg^{2+} uptake in breast cancer cells when bound to the protein tyrosine phosphatase of regenerating liver 2 (PRL-2)[47, 48]. CNNM4 is also related to cancer by PRLs, which have been reported to inhibit CNNM4's Mg^{2+}-efflux activity in order to raise cytosolic Mg^{2+} levels [57]. Thus, CNNMs have been implicated in both Mg^{2+} influx and efflux, and despite their physiological and pathological significance, their precise role and control remain unknown. Within the context of our study of the effect of intracellular Mg^{2+} on the cytoskeleton (Section 3, Experimental Results), we employed CNNM2's proven ability to lower intracellular Mg^{2+} to manipulate cytosolic Mg^{2+} and investigate Mg^{2+} effect on the cell cytoskeleton.

In Section 5 of the Experimental Results, we share the results of our investigation of the effect of the ARL15 protein on TRPM7 expression, cellular localization, and functional activity. ARL15 is a member of the family ADP-Ribosylation Factor (ARF) family of proteins, which is regulated by bound guanine nucleotides. ARF proteins function with guanine nucleotide exchange factors (GEF) and GTPase-activating proteins (GAP), which regulate GTP binding and hydrolysis, respectively. ARF proteins are known to control vesicle membrane trafficking and organelle structure. In

the endoplasmic reticulum, Golgi and plasma membrane, ARF proteins are found as dimers. There is evidence that membrane ARF proteins interact with membrane-localized proteins such as TRPM7. ARL15 belongs to ARF-like (ARL) proteins that have similar functions to ARF proteins but are thought to have broader roles. ARL proteins have not been extensively studied and the essential function of ARL15 has not yet been identified. Nevertheless, mutations in ARL15 have been associated with hypomagnesemia and ARL15 has been shown to regulate the TRPM6, a channel with significant sequence similarity to TRPM7[58].

7. Rationale

Evidence from many sources has shown that intracellular Mg^{2+} can affect the cytoskeleton. In addition, ROS is now recognized as a regulator of many proteins that influence cytoskeletal remodeling. We hypothesize, that changes in intracellular Mg^{2+} controls cytoskeletal remodeling through Mg^{2+} actions on intracellular ROS levels. The following thesis will present evidence in support of this hypothesis as well as report new discoveries regarding the regulation of the TRPM7 channel by CNNM and ARL15 proteins.

MATERIALS AND METHODS

1. Reagents

All chemicals, unless otherwise stated, were obtained from Sigma (St. Louis, MO). All of the cell culture reagents, unless otherwise stated, were purchased from Life Technologies (Carlsbad, CA). Tetracycline, carbenicillin, kanamycin, were purchased from Gold Biotechnology (St. Louis, MO).

2. Cell Lines

The TRPM7-knockdown fibroblast cell line (3T3-M7shRNA6) originated from Swiss 3T3 cells (American Type Culture Collection number: CCL-92) and was made by standard approaches using a previously characterized shRNA (shRNA6) that specifically target mouse TRPM7 [25]. Cells were cultured in Dulbecco's Modified Eagle's Medium (DMEM) with 10% fetal bovine serum (FBS), unless otherwise indicated. The methods used to create the cell lines and a description of their full characterization have been previously described[25]. The LTRPC7 cell line[2], which expresses FLAG-tagged mouse TRPM7 under tetracycline control (293-M7), was generously provided by Dr. Andrew Scharenberg (University of Washington), and was used to make the CNNM3 and CNNM4 knockout cell lines (described below). The tetracycline inducible 293-TRPM7 stable cell line, expressing HA-tagged TRPM7 (293-TRPM7) was generated using the Flp-In system (Thermo Fisher, CA), using the commercially available Flp-In T-Rex 293 cells as described in a previous study [17]. Transient transfections of the HEK-293 cell lines were performed using the Turbofect

transfection reagent (Thermo Fisher, MA), according to the manufacturer's protocol.

The Opossum kidney proximal tubule (OK) cell line was provided by Dr. Judith A. Cole from Department of Biological Sciences, the University of Memphis. The cells were cultured in DMED/F12 medium supplemented with 5% of FBS. Transfection of OK cells were carried out using Lipofectamine3000 (Thermo Fisher, MA), according to the manufacturer's protocol.

3. DNA Constructs

To make Adenovirus expressing hNOX1 and hCAT-10, ORFs DNA of NOX1 and CAT-10 were cloned by PCR by using forward primer for NOX1 5' – CAC CAT GGA CTA CAA GGA CGA CGA TGA CAA GAT GGG AAA CTG GGT GGT TAA C-3' and the reverse 5'– GCG GCC GCT CAA AAA TTT TCT TTG TTG AAG TAG AAT TG -3' and forward primer for CAT-10 5'– CAC CAT GGA CTA CAA GGA CGA CGA TGA CAA GAT GGC TGA CAG CCG GGA TCC C-3' and reverse 5' – GCG GCC GCT CAC AGA TTT GCC TTC TCC CTT GCC GCC AAG TG -3'. Next, we used the PCR product for cloning into Invitrogen Gateway® entry vector pENTR/D-Topo by Topo cloning and then used recombination to transfer the genes of interest to destination vector pAd/CMV.V5-DEST using the Gateway® LR clonase II Enzyme Mix with one shot® Omni Max™ 2T1 chemically competent cells (Invitrogen, CA). To make the recombinant adenoviruses expressing NOX1 and CAT individually, the Viral Power Adenoviral Expression System was used following the

manufacture's instruction. 293A cells were used to amplify the viruses. Plaque forming assay was applied to determined viral titers in 293A cells.

NOXO1 (MR205276) and NOXA1 (MR207092) were purchased from Origene Technologies, MD. We followed similar steps to generate recombinant adenovirus expression NOXO1 and NOXA1. The forward primer for NOXO1 was 5' – CAC CGG CAT GGC AAG CCC AAG ACA CCC ATG ATC AGC CCA T -3' and for the reverse, 5' - TTA AAC CTT ATC GTC GTC ATC CTT GTAATC CAG GAT ATC ATT TGC -3', and forward primer for NOXA1 was 5' – CAC CGG CAT GAG CTC TCT AGG GGA TCA GAT ACG GGA CTG G -3' and for the reverse 5' - TTA AAC CTT ATC GTC GTC ATC CTT GTAATC CAG GAT ATC ATT TGC -3.'

A pAd-CMV/V5-GW/LacZ and SLC41A2 were generated previously in our lab by using similar system and they were used as negative and positive controls respectively in this study [25].

4. Western Blotting**.**

293A cells were seeded at density around 1×10^6 cells in 60mm culture plate for 16-18 h. The next day when the cells reached 70-80 % confluent, the cells were transduced with the recombinant adenoviruses. After 24 h the cells were lysed with mild lysis buffer (50mM Tris (pH7.4), 150mM NaCl, 1 % IGEPAL) containing protease inhibitor cocktail (Sigma Aldrich, Mo). Proteins were detected using a standard protocol for Western blot. The Anti-FLAG antibody (Sigma-Aldrich, Mo) was used to detect NOX1, CAT, CNNM2, and SLC41A2 protein expression while monoclonal Anti-Myc (clone 9E10, Sigma Aldrich, Mo) was used to detect NOXO1

and NOXA1.

5. Cell spreading assay:

For rescue experiments using Nox1 and SLC41A1, R6, R6-Nox1 and R6-SLC41A2, cells were trypsinized after 3 days post viral transduction, and then resuspended in serum free DMEM containing 0.2% BSA at 37°C for 1 h and replated on culture dished coated with 10 $\mu g/cm^2$ fibronectin. Images of cell morphologies were obtained using an Olympus/CK2 microscope. The images were taking by Micro Max-CCD camera. Cells spreading quantification was analyzed by Fiji software by dividing the length on the cell by its width. The numbers of the cells counted were 150 cells for each experiment and each experiment was repeated at least 3 times.

For experiments employing recombinant adenoviruses expressing Catalase and CNNM2, 3T3, 3T3-LacZ, 3T3-CAT, 3T3-CNNM2, 3T3-free Mg^{+2} and 3T3-free Mg^{+2}-CNNM2 cells were seeded at approximately 0.1×10^6 in a 12 well culture plate. 24 h after viral transduction, the cell morphologies were analyzed by light microscopy as we can see the changing in length on width ratio.

6. Immunocytochemistry Analysis.

6.a: Overexpression of NOX1 and SLC41A2 in TRPM7 Knockdown Cells.

TRPM7 Knockdown cells were seeded in a 24 well plate at density of $0.1x10^6$ cells. The next day when the cells were 80-90 % confluent, they were individually transduced with adenovirus expressed Nox1, SLC41A2 and LacZ.

After 3 days, the cells were trypsinzed and replated onto fibronectin coated coverslips placed into the 24 wells plate. The following day the cells were washed two times with 1X PBS and fixed with 4 % paraformaldehyde in PBS for 20 min at room temperature. The fixed cells were permeabilized by using 0.1% Triton X-100 in PBS for 20 min at room temperature. Next, 5% FBS in PBS was used for blocking at 30°C for 1 h. After blocking, the cells were incubated in appropriate primary antibodies for 1 h at 30 °C. To detect filamentous actin, we used phalloidin at a dilution of 1:100. To detect tubulin, we used anti-tubulin (Sigma) (1:500 dilution). After three 5-min washing steps with 5% FBS in PBS, the Alexa Fluor™ 488 and Alexa Fluor™ 568 secondary antibodies (Thermo Fisher, MA) (1:2000 dilution) were applied, followed by 5 min incubation with DAPI (1:4000 dilution) at room temperature. After 3 washes with 5% FBS in PBS and 3 washes with PBS, the coverslips with cells were mounted onto glass slides with Aqua Poly/Mount (Polyscience, Inc). Images were taken by a Yokogawa CSUX1-5000 microscope under 63X magnification using 488 nm and 561 nm wavelengths at the Rutgers RWJMS CORE Confocal facility.

6.b: Overexpression of CAT and CNNM2 in 3T3 Fibroblasts

3T3 cells were seeded onto Poly-L-Lysine (Sigma-Aldrich, Mo) coated coverslips placed into 24 well plates at density $0.1x10^6$. The following day, when the cells were 60-70 % confluent, they were virally transduced individually with recombinant adenovirus expressing CAT and CNNM2. After 24 h, the cells were washed two times with 1X PBS and fixed with 4 % paraformaldehyde in PBS for 20 min at room temperature. To complete the staining, we applied similar

immunocytochemistry steps to those described above.

6.c: Localization of TRPM7 and ARL15 in 293-TRPM7 cells

293-TRPM7 cells, which express HA-TRPM7 in response to tetracycline (TET), were seeded at a density of 0.2 x 10^6 onto Poly-L-Lysine (Sigma-Aldrich, Mo) coated coverslips placed in 24 well plates. The cells were transfected with 5 μg ALR15 the next day when the cells were at 70 % confluence; 5μg/ml tetracycline was added 3 hours post-transfection to induce TRPM7 expression. 48 hours after transfection, cells were washed twice with 1X PBS and fixed for 20 minutes at room temperature with 4 % paraformaldehyde in PBS. The fixed cells were permeabilized for 20 minutes at room temperature with 0.1 % Triton X-100 in PBS, accompanied by 1 hour of blocking at 30 °C with 5 % FBS in PBS. For 1 hour, the cells were stained with anti-HA antibody to detect TRPM7 and the anti-FLAG antibody to detect ARL15, using DAPI to stain the nucleus. Keeping the temperature at 30°C, we processed the coverslips with secondary antibodies for 1 hour. After 3 washes with 5% FBS in PBS and 3 washes with PBS, the coverslips with cells were mounted onto glass slides with Aqua Poly/Mount (Polyscience, Inc) and imaged as described above.

6d: Localization of TRPM7 and ARL15 in OK cells

1 x 10^5 OK cells were seeded onto glass coverslips placed into 24-well plates 24 h before transfection was performed. To study the localization of TRPM7 and ARL15, OK cells were transfected with 0.4 μg HA-TRPM7 and 0.4 μg FLAG-ARL15. 48 h post-transfection, cells were fixed using 4 % paraformaldehyde in PBS for 20 min at room temperature. 0.1% Triton X-100 in PBS were used to

permeabilized the cells at 30 °C for 10 min and then 5% FBS in PBS were used for blocking at 30 °C for 30 min. Then cells were incubated in appropriate primary antibodies for 1 h at 30 °C. To detect HA-TRPM7 we used a rat monoclonal antibody anti-HA antibody (3F10; Roche Life Sciences, IN) (1:1000 dilution). To detect FLAG-ARL15, we used anti-FLAG monoclonal antibody from Sigma. After three 5-min washing steps with 5% FBS in PBS, Alexa Fluor™ 488 and Alexa Fluor™ 568 were used as secondary antibodies (Thermo Fisher, MA) (1:2000 dilution), then followed by 5-min incubation of DAPI (1:4000 dilution) at 30 °C. After 3 washes with 5% FBS in PBS and 3 washes with PBS, the coverslips with cells were mounted onto glass slide with Aqua Poly/Mount (Polyscience, Inc). Images were taken by a Yokogawa CSUX1-5000 microscope under 63X magnification using 488 nm and 561 nm wavelengths at the Rutgers RWJMS CORE Confocal facility.

7. Immunoblotting.

For biochemical experiments to analyze FAK and Src phosphorylation during cell spreading, 3T3, 3T3-CAT, 3T3-CNNM2, cells were trypsinized and resuspended in serum free DMEM containing 0.2 % BSA at 37°C for 1 h and replated on culture dished coated with 10 μg/cm^2 fibronectin. After 20 min incubation at 37°C, the cells were lysed by adding 150 μl 2X SDS sample buffer and the samples were then processed using a standard Western blotting protocol. Anti-FAK, pFAK Y397, Src and pSrc Tyr416 (Cell Signaling) were used as the primary antibodies. Anti-β-Actin (Santa Cruz biotechnology) was used to probe

actin levels as a loading control in the immunoblots of FAK while anti Vinculin antibody was used as loading control for the immunoblots of Src. Super Signal West Pico and Western Bright™ Quantum (Thermo Fisher Scientific) were used for immunochemiluminescence detection.

For the experiments analyzing the effect of ARL15 on TRPM7 protein expression (EXPERIMENTAL RESULTS, Section 5) 293-TRPM7 cells expressing HA-TRPM7 were seeded at a density of about $1x10^6$ in a 60 mm culture plate. The cells were transfected with various amounts of ARL15 the next day, after the cells have achieved 70-80 % confluence. After 24 hours, the cells were lysed with a mild lysis buffer (50mM Tris (pH7.4), 150mM NaCl, and 1% IGEPAL) containing a protease inhibitor mixture (Sigma Aldrich, Mo). The rat monoclonal anti-HA antibody (Roche) was used to detect HA-TRPM7. The ARL15 antibody, described above, was used to detect ARL15 using the normal Western blot protocol. Vinculin, used as a loading control, was detected by Western blot using an anti-vinculin antibody (Sigma).

8. Immunoprecipitation Experiment with TRPM7 and ARL15

293-TRPM7 cells were seeded at a density of about 3×10^6 in a 100 mm culture plate. After 16-18 hours, the cells were transfected with 5 μg ARL15. The next day, when the cells were 70-80 percent confluence, tetracycline (TET) was applied after 2-3 hours to induce TRPM7 expression. Following 24 hours of TRPM7 induction, the cells were lysed with 1 ml of mild lysis buffer as described above. The supernatant was then incubated overnight with HA beads (Sigma) to

immunoprecipitated HA-TRPM7. Following the washing of the beads, 1X SDS sample buffer was applied, and the sample was heated for 5 minutes to elute the proteins from the beads. The samples were then resolved using SDS-PAGE. The TRPM7 protein detected using an anti-HA antibody, and ARL15 was detected using an anti-ARL15 antibody. As a loading control, protein samples were probed using and an anti-vinculin antibody.

9. ROS Measurement.

Intracellular ROS levels were measured using a molecular probe called 2',7'-dichlorodihydrofluorescein diacetate (CM-H2DCFDA) (Invitrogen, C6827). For these experiments, the cells were seeded on poly-lysine coated 24 wells at a density $0.1x10^6$ cells/wells. Next day, when the cells were 70 % confluent, cells were transduced with the recombinant viruses. After a certain time, depending on the changes caused by individual viruses, the cells were labelled with 2 μM H2DCFDA. For example, cells transduced with recombinant adenoviruses for NADPH oxidase (Nox1) and SLC41A2 were labelled with 2 μM H2DCFDA after 3 days and, whereas for cells transduced with CAT and CNNM2 adenoviruses they were labeled after 2 days. Following a 30 min incubation with the probe, the cells were washed 3 times with HBSS buffer to remove the ROS indicator. Finally, the cells were incubated in HBSS buffer and the fluorescent intensity of the probe was visualized using an inverted Olympus IX70 fluorescence microscope. ImageJ software was used to measure the fluorescent intensity. 50 cells were counted for each experimental sample.

10. Measurement of Intracellular Mg^{2+}.

To determine whether the Mg^{2+} transporter (SLC41A2) and NOX1 increase intracellular levels of Mg^{2+} in TRPM7 knockdown cells and the CNNM2 protein decreases Mg^{2+} levels in Swiss fibroblast WT cells, but CAT does not, we measured Mg^{2+} levels using Molecular Probes Mg^{2+} indicator Mag-Fluo-4, which is very sensitive to Mg^{2+} concentrations ranging from 0.1 to 10 mM . Briefly, TRPM7 knockdown cells and 3T3 wild type (WT) cells were seeded in polylysine coated 24 wells at density $0.1x10^6$ cells/well. After each indicated viral transduction, the cells were labelled with Mg^{2+} indicators Mag-Fluo-4 (2.5 μM) following manufacturer instructions (Thermo Fisher Scientific, M14206). Following 30 min of incubation, the cells were washed 2 times and incubated with HBSS. The images were acquired using an inverted Olympus IX70 fluorescence microscope. Image J software was used to measure the fluorescent intensity in individual cells. 50 cells were counted for each experimental sample.

11. CNNM3 and CNNM4 Knockout Cell Lines

The LTRPC7 cells lines expressing TRPM7 (293-M7) and deficient in *CNNM3*, *CNNM4*, or *CNNM3* and *CNNM4* (293-M7-ΔCNNM3, 293-M7-ΔCNNM4, 293-M7-ΔCNNM3/4 cells) were created using the Alt-R CRISPR-Cas9 System from Integrated DNA Technologies (Caralville, Iowa). The Alt-R CRISPR-Cas9 guide RNAs for CNNM3 and CNNM4 were 5'-AltR1/rArUrGrGrUrUrGrUrArGrArArArCrGrArGrUrGrArGrUrUrUrUrArGrArGrCrUr

ArUrGrCrU/AltR2/-3' and 5'-/AltR1/rCrArArGrUrCrGrUrGrUrGrGrGrArCrGrArArCrCrGrUrUrUrUrArGrArGrCrUrArUrGrCrU/AltR2/-3. The guide RNAs were transfected into LTRPC7 cells with Alt-R CRISPR crRNA, Alt-R CRISPR-Cas9 tracrRNA and recombinant Alt-R S. pyogenes Cas9 Nucleus V3. Two days following transfection, the cells were serially diluted. Colonies were screened for loss of protein expression using antibodies specific for CNNM3 (NBP2-32134, Novus Biologicals) and CNNM4 (ab191207; Abcam).

12. Zinc-influx assay

We adapted a protocol from the one employed by Inoue and colleagues to monitor Zn^{2+}-influx by TRPM7 [59]. Briefly, cells were labeled with the Zinc indicator Fluo-Zin-3 (2.5 μM) following manufacturer instruction (Thermo Fisher Scientific). The cells were then incubated with Hanks Balanced Salt Solution (HBSS) containing 30 μM $ZnCl_2$ for 5-10 minutes and then images were acquired on an inverted Olympus IX70 fluorescence microscope. Fluorescence intensity of individual cells was measured using Fiji [60]. 50 cells were counted for each experimental sample.

13. Electrophysiological Recordings

The voltage-clamp technique was used to evaluate the whole-cell currents of TRPM7 expressed in HEK-293 cells as described [61]. Briefly, whole-cell current

recordings of TRPM7-expressing cells were elicited by voltage stimuli lasting 250 ms delivered every 1 second using voltage ramps from –100 to +100 mV. Data was digitized at 2 or 5 kHz and digitally filtered off-line at 1 kHz. The internal pipette solution for macroscopic current recordings contained (in mM) 145 Cs-methanesulfonate, 8 NaCl, 10 EGTA, and 10 HEPES, pH adjusted to 7.2 with CsOH. The extracellular solution for whole-cell recordings contained (in mM) 140 NaCl, 5 KCl, 2 $CaCl_2$, 10 HEPES, and 10 glucose, pH adjusted to 7.4 (NaOH). For rescue experiments, transient transfection pCMV-4A-CNNM4 expressed CNNM4 at high levels, which reduced TRPM7 protein expression, making measurement of whole cell currents too variable. To overcome this problem, pCuO-MCS-CNNM4-FLAG was employed for sustained modest re-expression of CNNM4 in 293-M7-ΔCNNM3/4 cells, with CNNM4 expression induced upon application of cumate to the cell media. To achieve sustained episomal expression, cells transfected with pCuO-MCS-CNNM4-FLAG were selected by application of puromycin to the growth media. The surviving cells were used for the rescue experiments.

14. Cell Surface Biotinylation

Cell surface proteins were biotinylated for 30 min at 4°C in 0.5 mg/mL sulfo-NHS-LC-LC-biotin (Pierce, Rockford, IL, USA). Cells were washed and lysed in lysis buffer. 10% (v/v) of the sample was taken as input control and the rest of the protein lysates were incubated overnight with ANTI-FLAG-M2 Affinity Gel (Sigma-Aldrich) at 4°C. The next day, unbound protein was discarded by washing the beads three times with lysis buffer. The remaining protein lysates were denatured in Laemmli

containing 100 mM DTT for 30 min at 37°C and subsequently subjected to SDS-PAGE. Anti-Flag Antibody (Sigma) was used to detect whole FLAG-TRPM7 pulled down and Avidin-HRP Conjugate (Bio-Rad) was used to detect the biotin-labeled surface FLAG-TRPM7 protein amount.

15. Statistical analysis.

The *P* values were calculated by using two-tail Student's t-test and ANOVA methods. $P < 0.05$ (*) or < 0.01 (**) are considered significantly different.

EXPERIMENTAL RESULTS

SECTION 1: Changing Intracellular Mg^{2+} and ROS Causes Changes in Cell Morphology.

1-1 Increasing Cellular ROS Levels Rescues Cell Morphology of TRPM7-Knockdown Cells.

In a previous study by the Runnels lab, it was shown that knockdown of TRPM7 in Swiss 3T3 fibroblasts (CRL-92) causes a defect in cell morphology and cell migration [25]. Interestingly, the defects could be rescued by overexpression of the magnesium transporter SLC41A2, indicating a role of Mg^{2+} in TRPM7 function. In a separate study, it was found that levels of ROS are lower in TRPM7-knockdown fibroblasts compared to control cells [32]. Moreover, it was discovered that the overexpression of SLC41A2 was able to increase cellular ROS levels in TRPM7 knockdown cells. ROS function as signaling molecules that regulate many cellular functions, including cell morphology and migration [35, 62]. We hypothesized that the defect in cell morphology caused by knockdown of TRPM7 may be due to decrease in cellular ROS levels caused by a decrease in the intracellular concentration of Mg^{2+}. Therefore, we tested whether increasing ROS levels in TRPM7 knockdown cells could restore the defect in cells morphology caused by depletion of the channel. To increase cellular ROS levels, we co-expressed NADPH oxidase (NOX1) with its co-subunits NOXO1 and NOXA1, which are required for full NADPH oxidase activity [63]. Overexpression of NOX1 in TRPM7 knockdown cells restored the morphology to a WT cell shape as effectively as

overexpression of SLC41A2, which we employed as a positive control in our experiments (Figure 4A). As expected, overexpression of LacZ had no effect on cell morphology, intracellular Mg^{2+}, or ROS levels (Figure 5B), indicating that the changes we observed with NOX1 and SLC41A2 are not due to the use of a recombinant adenovirus for protein expression. To confirm that overexpression of NOX1 increases cellular ROS level independent of any changes in cellular Mg^{2+} levels, we used a magnesium concentration assay to test the Mg^{2+} level after overexpression NOX1, which we found was unchanged (Figure 5A). As expected, overexpression of SLC41A2 in TRPM7 knockdown cells increased cellular Mg^{2+} levels (Figure 5A). In addition, overexpression of NOX1 and SLC41A2 also increased cellular ROS levels (Figure 5B).

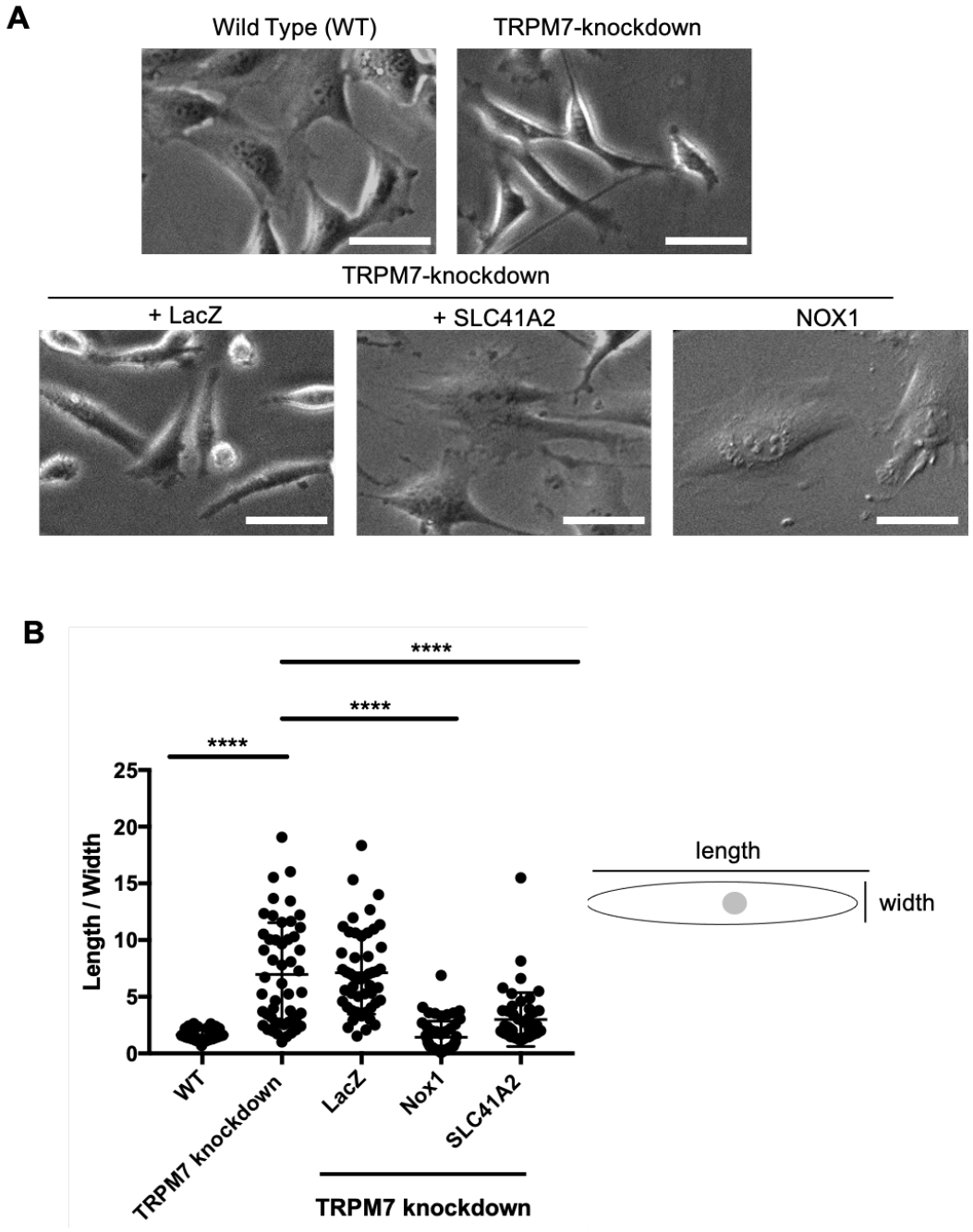

Figure 4: Effect of SLC41A2 and NOX1 on cell morphology.

(A) Adenoviral expression of SLC41A2 in stable TRPM7 knockdown in Swiss 3T3

fibroblasts rescued the cell morphology defect, causing cells to become more spread compared to the TRPM7 knockdown cells. Similarly, TRPM7 knockdown cells co-transduced with NOX1, NOXA1 and NOXO1 also restored the defect in cell morphology caused by TRPM7 depletion. In both cases, the cells were transduced with the viruses and after 3 days the cells were trypsinyzed and re-plated to monitor the cell morphology the next day using phase-contrast light microscopy. White scale bar = 100 μm. (B) We quantified the change in cells morphology by measuring the ratio of the cell's length to its width. TRPM7 knockdown cells have a defect characterized with very long shape that make the cells length much larger than its width. We applied one way ANOVA to compare between the groups to WT cells. For each group, 50 cells were counted, and the experiment was repeated 3 times.

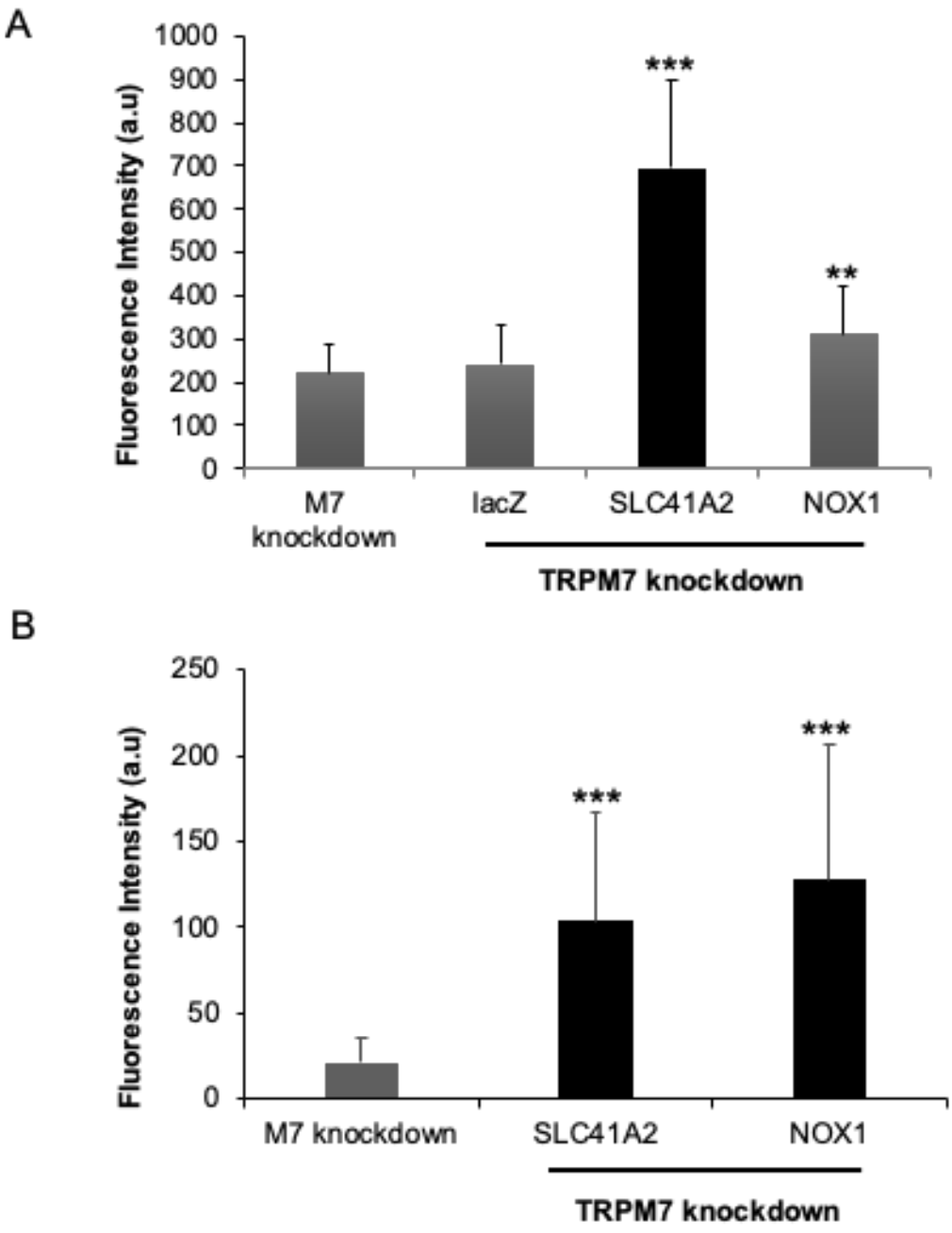

Figure 5: Expression of SLC41A2 increases Mg^{2+} and ROS levels while the expression of NOX1 increases ROS levels in TRPM7 knockdown cells.

(A)TRPM7 knockdown 3T3 cells have lower Mg^{2+} level and expression of SLC41A2 increased cellular Mg^{2+} levels in TRPM7 knockdown 3T3 as quantified

using the Mg^{2+} indicator Mag-Fluo-4. TRPM7 knockdown cells were seeded in 24 wells and the next day were virally transduced with LacZ, SLC41A2 or the NOX1 complex (NOX1, NOXA1, NOXO1) recombinant adenovirus. After 3 days, the cells were washed with HBSS and treated with Mg^{2+} indicator Mag-Fluo-4 (2.5 μM) for 30 min and washed again 3 times. The cells were kept in HBSS buffer to monitor the fluorescent intensity of the probe by fluorescence microscopy. Fiji software was used to quantify the fluorescence intensity of each cells. 50 cells were counted for each group. One way ANOVA test was used for the statistical analysis. * $p < 0.05$, ** $p < 0.01$. (B)TRPM7 knockdown 3T3 cells virally transduced with either the recombinant SLC41A2 or the NOX1 complex recombinant adenovirus exhibited significantly higher intracellular ROS levels compared to TRPM7 knockdown cells. TRPM7 knockdown cells were seeded in 24 wells plate and transduced with the SLC41A2 and Nox1 complex (NOX1, NOXA1, NOXO1) recombinant adenovirus, with non-transduced cells serving as a negative control. Three days after viral transduction, the cells were labeled with the ROS indicator 2',7'-dichlorodihydrofluorescein diacetate (CM-H2DCFDA) and the fluorescence intensity was measured by fluorescence microscopy. The data were analyzed by Fiji software. 25 cells were counted for each group. One way ANOVA test was used for the statistical analysis. * $p < 0.05$, ** $p < 0.01$.

1-2 Decreasing Cellular ROS Levels or Lowering Cellular Mg^{2+} Produces a Spindle-like Morphology in Wildtype Swiss 3T3 Cells.

In section 1-1 we reported experiments showing that overexpression of SLC41A2 or NOX1 rescues the cell morphology caused by depletion of TRPM7. We next investigated whether lowering cellular ROS levels would produce the same change in morphology that occurred when TRPM7 was depleted from cells (i.e. a change from a spread to a long spindle morphology). To lower cellular ROS levels, we overexpressed catalase using a recombinant adenovirus containing the cDNA for human catalase (Ad-CAT1), which has been previously employed to convert H_2O_2 to H_2O and O_2 in cells [64, 65]. Viral transduction of WT fibroblasts with Ad-CAT1, but not the negative control Ad-LacZ, caused cells to begin to change shape within 4 hours. After 24 hours, cells had a spindle-like morphology similar to TRPM7-knockdown cells (Figure 6A). We tested whether CAT1 had any effect on intracellular Mg^{2+} levels and found that viral transduction of CAT1 had no effect on the concentration of cytosolic free Mg^{2+} (Figure 7A). These results indicate that lowering cellular ROS levels is sufficient to change the cell morphology independent of any changes in intracellular Mg^{2+} levels. In section 1-1 we showed that overexpression of SLC41A2 in TRPM7-knockdown cells raises intracellular Mg^{2+}, which in turn raises intracellular ROS levels. To test whether lowering intracellular Mg^{2+} would cause the opposite effect and lower ROS levels we used viral expression of CNNM2 as a tool to lower the concentration of cytosolic free Mg^{2+}. CNNM2 functions as a Mg^{2+}-exporter. When overexpressed in cells CNNM2 stimulates the lowering of cytosolic free Mg^{2+} [45]. Viral transduction of CNNM2 (Ad-

CNNM2) into WT fibroblasts also transformed cells from a spread to spindle morphology within 24-48 hours (Figure 8A). As expected, viral transduction of LacZ did not change the cell morphology of WT cells. When we measured cellular Mg^{2+} in CNNM2-expressing cells we observed lower Mg^{2+} levels compared to WT cells expressing LacZ (Figure 9A). Importantly, expression of CNNM2 caused a decrease in intracellular ROS levels (Figure 9B). These results indicate that lowering cellular Mg^{2+} independent of TRPM7 disrupts cell morphology. Thus, it is the change in Mg^{2+}, rather than the identity of the magnesium transporter, that is responsible for the disruption in cell morphology. Our results also indicate that intracellular Mg^{2+} is an important determinant of cellular ROS levels, which our experimental data demonstrate have a profound effect on cell morphology. These results suggest that Mg^{2+} and ROS together produce their effects by influencing the cell's cytoskeleton.

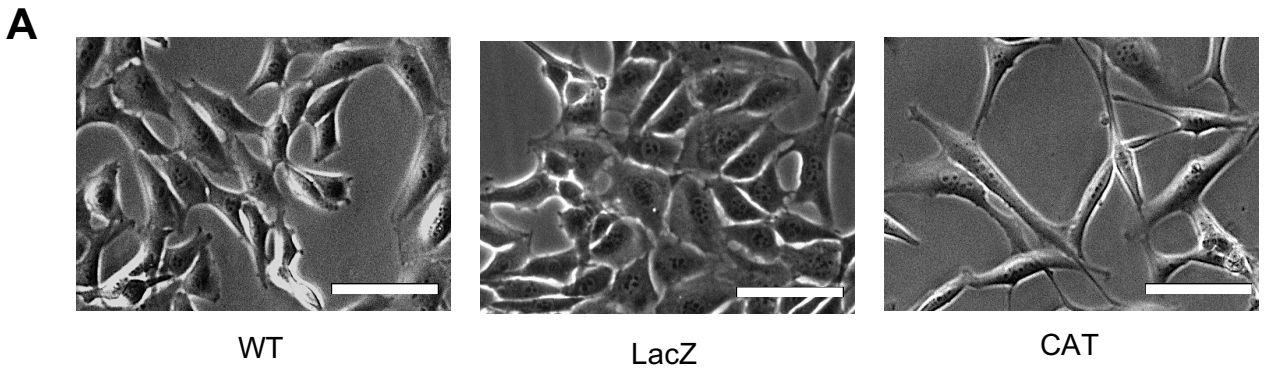

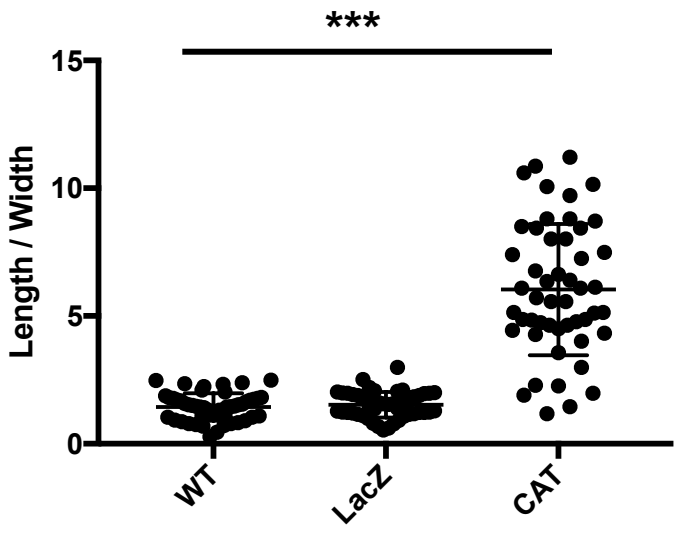

Figure 6: Effect of Catalase on Cell Morphology.

(A) Viral transduction of wild type (WT) Type 3T3 fibroblasts with a recombinant adenovirus expressing CAT caused a change in cell shape, causing cells to become thin and long compared to control (non-transduced cells). By contrast, viral expression of LacZ, the negative control, had no effect on cell morphology. In this experiment, the cells were seeded in 24 well plates and next day, when the cells reached to 60% confluency, the cells were virally transduced with the CAT1

adenovirus. Notably, a dramatic change in cell morphology became evident after 24 hrs. White scale bar = 100 μm. (B) Quantification of the change in the cell morphology was accomplished by measuring the ratio of the length to the width of cells. The defect in cell morphology is characterized with very long shape that make the cells length longer than its width. We applied one way ANOVA to compare between the groups and non-transduced WT cells. For each group, 50 cells were counted, and each experiment was repeated 3 times.

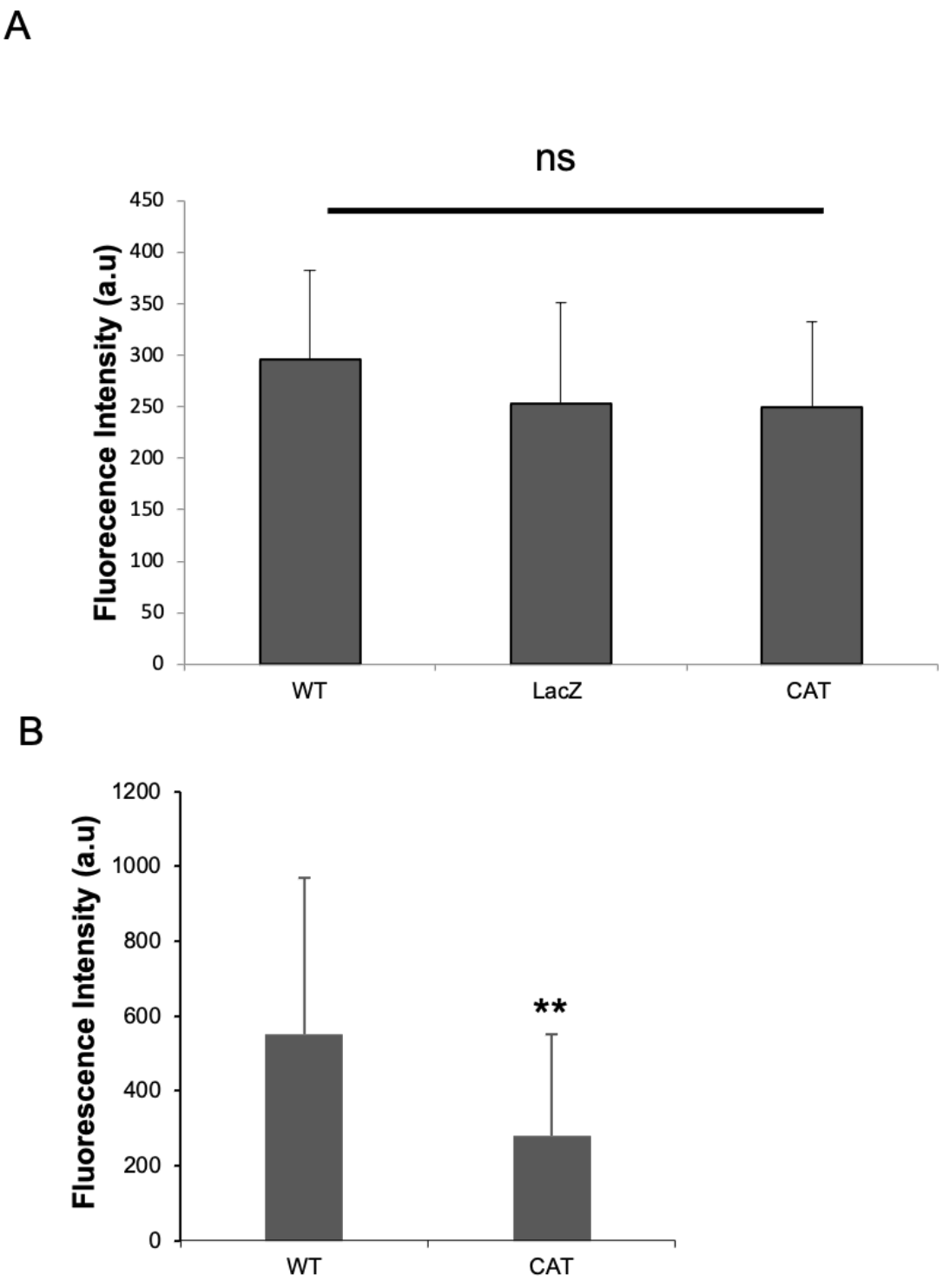

Figure 7: Catalase decreases intracellular ROS levels but not Mg^{2+} levels.

(A) The Mg^{2+} levels of Swiss 3T3 fibroblasts virally transduced with a recombinant adenovirus expressing CAT1 showed were not significantly compared to wild type

cells (WT) or negative control cells transduced with a recombinant adenovirus expressing LacZ. To measure intracellular Mg^{2+} levels, the cells were seeded in a 24 well plate. 24 hours after viral transduction, cells were labeled with the Mg^{2+} indicator Mag-Fluo-4 (2.5 μM) for 30 min and washed 3 times. The cells were incubated in HBSS buffer and the cell's fluorescent intensity was measured by fluorescent microscopy. Fiji software was employed to analyze the data. 50 cells were counted for each group. One way ANOVA test was used for the statistical analysis. (B) Swiss 3T3 fibroblasts virally transduced with recombinant adenovirus expressing CAT had significantly lower intracellular ROS levels compared to cells virally transduced with a LacZ adenovirus. The cells were seeded in a 24 wells plate and 24 hours after viral transduction the cells were labeled with the ROS indicator 2',7'-dichlorodihydrofluorescein diacetate (CM-H2DCFDA) and the cellular fluorescence intensity was detected by the fluorescence microscopy. The data were analyzed by Fiji software. 25 cells were counted for each group. A Two-tailed Student's T test was used for the statistical analysis. ** $p < 0.01$.

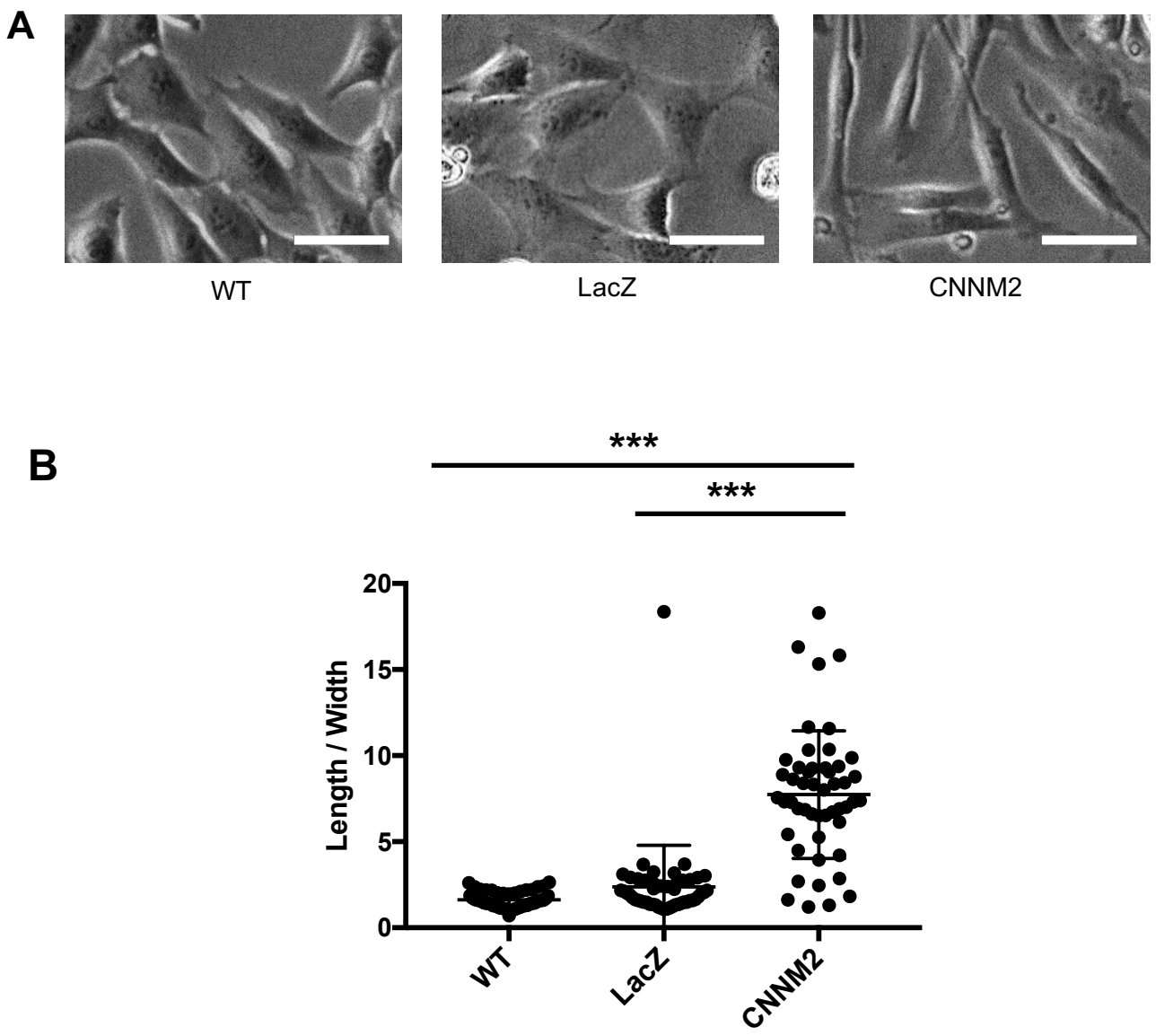

Figure 8: Effect of CNNM2 on Cell Morphology.

(A) Viral transduction of Swiss 3T3 fibroblasts with a recombinant adenovirus expressing CNNM2 caused a defect in cell morphology, with the cells became longer and less spread. In contrast, fibroblasts transduced with a recombinant adenovirus expressing LacZ had a similar cell morphology to wildtype (WT) cells. In this experiment the cells seeded were in a 24 wells plate. Twenty-four hours after viral transductions, images were taken by phase-contrast light microscopy to

compare the cells morphology between the different cell groups. White scale bar = 100 μm. (B) Quantification of the change in the cell morphology by measuring the ratio of the cell length to its width. The cell morphology defect produced by cells expressing CNNM2 is characterized with cells that have a long spindle shape. For each group, 50 cells were counted, and each individual experiment was repeated 3 times. One way ANOVA test was used for the statistical analysis. *** $p < 0.01$.

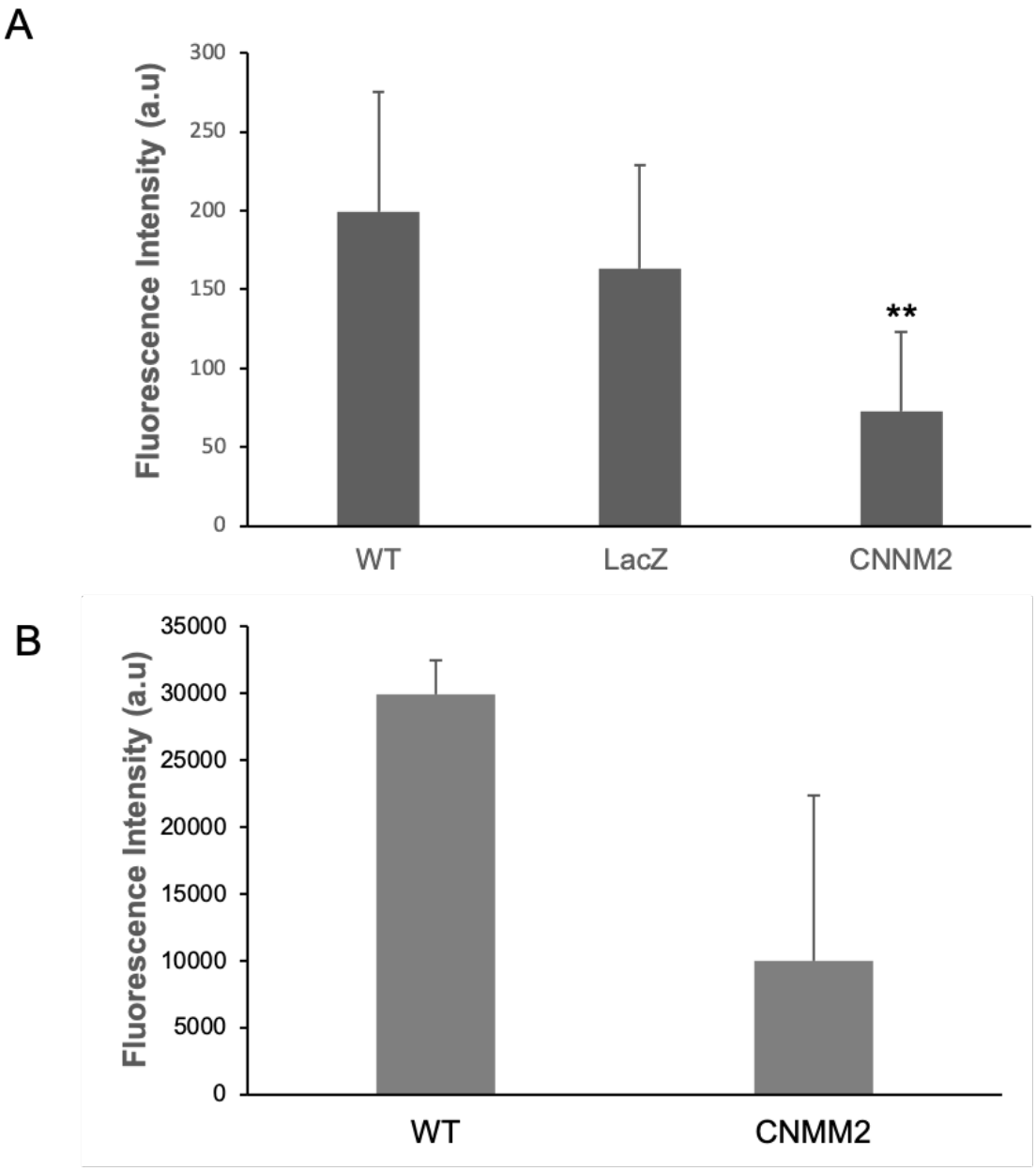

Figure 9: CNNM2 overexpression decreased the Mg^{2+} and ROS levels in WT Fibroblasts.

(A) Swiss 3T3 fibroblasts virally transduced with the recombinant CNNM2 adenovirus have significantly lower Mg^{2+} levels than the control non-virally

transduced WT cells, whereas cells expressing LacZ had no change in Mg^{2+}levels. The fibroblasts were seeded in 24 wells plate and 24 hours after viral transduction with the CNNM2 recombinant adenovirus, the cells were labeled with the Mg^{2+} indicator Mag-Fluo-4 (2.5 μM) for 30 min and washed 3 times with HBSS buffer before imaging by fluorescence microscopy. Fluorescent intensity was measured by the Fiji software. 50 cells were counted for each group. One way ANOVA test was applied to compare the groups. (B) Fibroblasts transduced with the recombinant CNNM2 adenovirus have significantly lower levels of ROS levels than wildtype fibroblasts or fibroblasts transduced with the LacZ adenovirus. The fibroblasts were seeded in 24 wells plate and 24 hours afterwards were virally transduced with the CNNM2 recombinant adenovirus. The cells were then labeled with ROS indicator 2',7'-dichlorodihydrofluorescein diacetate (CM-H2DCFDA) and the fluorescence was detected by the fluorescence microscopy. The fluorescent intensity was analyzed by Fiji software. 25 cells were counted for each group. Two-tailed Student's T test was used for the statistical analysis. * $p < 0.05$, ** $p < 0.01$.

SECTION 2. Changing of Intracellular Mg^{2+} And ROS Levels Causes Changes in Actin Stress Fiber Formation.

2-1 The Impact of Intracellular Mg^{2+} And ROS Levels on The Actin Cytoskeleton

We next tested how manipulating cellular Mg^{2+} and ROS affects the cytoskeleton. Overexpression of SLC41A2 is able to increases actin polymerization in TRPM7-knockdown cells. However, no obvious change in the structure of microtubules was observed when comparing TRPM7 knockdown cells to cells overexpressing SLC41A2 (Figure 10). Interestingly, overexpression of NOX1 in TRPM7 knockdown cells also resulted in more actin stress fibers (Figure 10) but had no effect on the tubulin cytoskeleton. These results suggest that changes in cell morphology in response to overexpression of SLC41A2 and NOX1 is driven by changes to actin cytoskeleton.

We then tested whether lowering cellular ROS using viral transduction of catalase (Ad-CAT1) would disrupt the cytoskeleton. Expression of CAT1 in WT fibroblasts, but not the negative control LacZ, reduced the amount of stress fibers and increased the amount of cortical actin in cells without affecting microtubule structures. These results indicate that ROS is required for regulation of the actin cytoskeleton. To test the effect of lowering intracellular Mg^{2+} we virally expressed CNNM2 in WT fibroblasts. Expression of CNNM2, which we showed lowers intracellular Mg^{2+} (Figure 9A), also caused a disruption of actin stress fibers similar to what we observed when CAT1 was overexpressed in fibroblasts (Figure 11). As expected, expression of LacZ in cells caused no change in the amount of actin stress fibers compared to non-transduced WT control cells. Collectively, these

results indicate that the change in cell morphology caused by changes in intracellular Mg^{2+} and ROS are due to alteration in the actin cytoskeleton and not to microtubules.

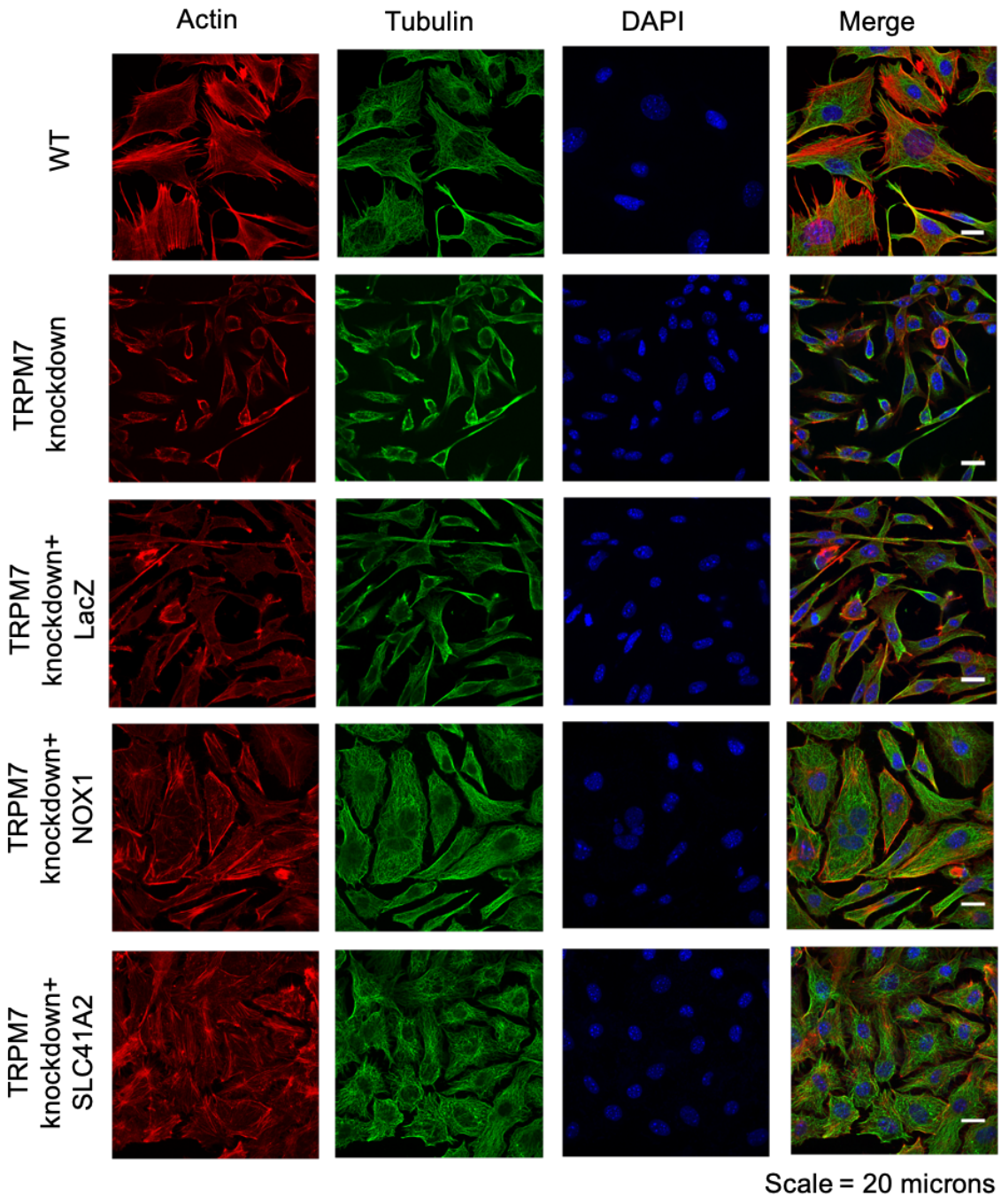

Figure 10: Overexpression of SLC41A2 and NOX1 Restore Actin Cytoskeletal Organization in TRPM7-Knockdown Cells.

Confocal images of phalloidin staining of filamentous actin and microtubules in TRPM7 knockdown cells, SLC41A2 virally transduced TRPM7 knockdown cells

and NOX1 virally transduced TRPM7 knockdown cells. The cells were stained by immunocytochemistry 72 hours after viral transduction and then were replated onto polylysine coated coverslip in 24 wells plate to stain the actin filaments by Phalloidin (green), α-tubulin by antibody staining (red), and DAPI (blue) to stain the nucleus. TRPM7 knockdown cells have less stress fibers and more actin localized to the cortical regions. No obvious disruption of the microtubule network was observed. Overexpression of SLC41A2 and NOX1 in TRPM7 knockdown cells restored stress fiber formation. Overexpression of LacZ had no effect on the cytoskeleton and was used as a negative control.

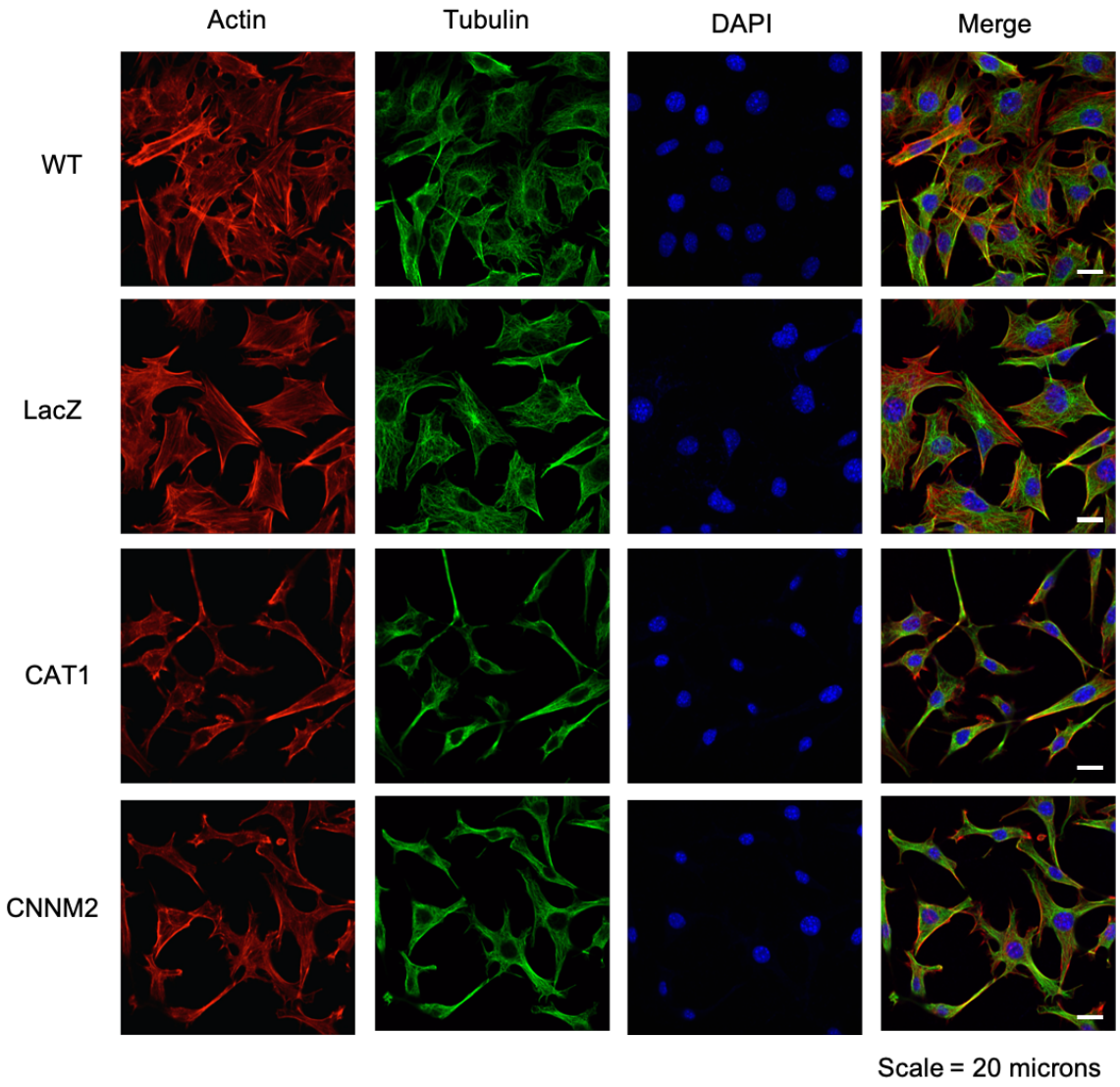

Figure 11: CAT and CNMM2 Disrupt Actin Stress Fibers but not Microtubules. Confocal images of phalloidin staining of filamentous actin and microtubules in wildtype Swiss 3T3 fibroblasts, and in CAT and CNNM2 virally transduced wildtype (WT) Swiss 3T3 fibroblasts. 24 hours post viral transductions, the cells were fixed and stained with phalloidin to detected filamentous actin (red), with antibodies recognizing α-tubulin (green), and with the nuclear stain DAPI (blue). Both

overexpression of CAT and CNNM2 in Swiss 3T3 fibroblasts disrupted stress fiber formation and increased cortical actin staining but did not cause any change in tubulin cytoskeleton. Overexpression of LacZ, as a negative control, in Swiss 3T3 fibroblasts had no effect on cytoskeletal structures.

SECTION 3. The Impact of Intracellular Mg^{2+} And ROS Levels on the FAK and Src Kinases Activity.

3-1 FAK & Src Kinase Activities Are Not Disrupted by CNNM or CAT Overexpression in WT Swiss 3T3 Cells

We've shown that overexpression of CNNM2 and CAT1 in WT Swiss 3T3 cells causes dramatic changes in cell morphology (Figure 6A,8A) as well as in the actin cytoskeleton (Figure 11). ROS can modulate the activities of numerous proteins involved in control of the cytoskeleton through their action of tyrosine phosphatases, whose activities are dependent on the redox state of a low pKA active site cysteine [38]. Inhibition of tyrosine phosphatases by oxidation prolongs the phosphorylation state of many phosphoproteins, include FAK and Src, which regulate the cytoskeleton [38, 66]. We thus conducted experiments to test whether overexpression of CNNM2 and CAT1 in WT Swiss 3T3 cells interferes with the activation of FAK and Src during cell spreading onto fibronectin-coated plates. As shown in Figure 13, the activation of FAK and Src, as visualized by their phosphorylation on Tyrosine 397 for FAK and Tyrosine 416, was not significantly affected by overexpression of CNNM2 or CAT1. This data indicates that the changes in ROS caused by CAT1 and CNNM2 and the resultant changes in cell

morphology and the cytoskeleton do not appear to be driven by FAK or Src kinases.

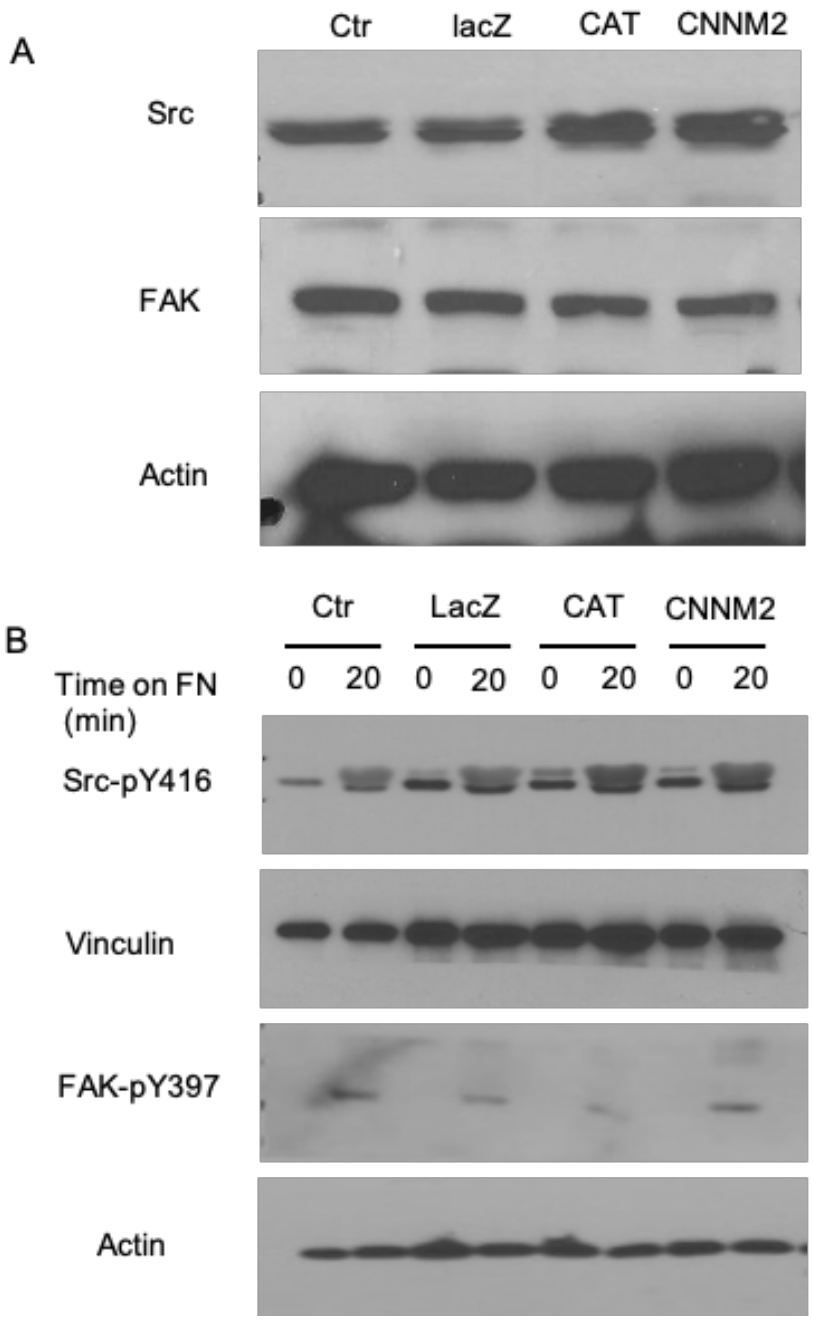

Figure 12: Overexpression of CAT and CNNM2 do not affect FAK and Src Kinases Activity.

(A) Overexpression of CAT and CNNM2 had no effect on the FAK and Src expression. The 3T3 cells were infected with a recombinant adenovirus expressing

CAT or CNNM2, and after 24 hrs. the cells were lysed to assess the protein levels by immunoblotting by using antibodies targeting FAK and Src. (B) Overexpression of CAT and CNNM2 had no effect on the FAK and Src activity. The 3T3 cells were infected with a recombinant adenovirus expressing CAT or CNNM2, and after 24 hrs. the cells were trypsinzed and suspended for one hour and replated to fibronectin coated 35 cm dish. The cells were incubated in 37˚C for 20 minutes. After 20 mins, the cells were lysed by adding 2X sample buffer to collect the attached cells. We assessed the phosphorylation of FAK and Src kinase using SDS-PAGE and Western Blot using primary antibodies recognizing FAK-pY397 and Src-pY416, which are the activated form of these kinases. We measured protein levels of vinculin as a loading control with Src kinase and actin as a loading control for FAK kinase.

SECTION 4. TRPM7 Regulation by CNNMs.

4.1 CNNMs interact with TRPM7 and Regulate its Activity.

To discover new TRPM7 ion channel regulators, the Runnels lab used mass spectrometry to examine FLAG-tagged mouse TRPM7 from a tetracycline-inducible HEK-293 cell line that was holding in the absence of tetracycline to maintain channel expression low (43). CNNM3 and CNNM4 were revealed to be possible TRPM7-interacting proteins by proteomic review.

Since CNNM3 and CNNM4 were the CNNM isoforms most frequently reported as interacting with TRPM7 in our mass spectrometry results, we wondered if endogenous CNNM3 and CNNM4 were needed to control TRPM7

channel function. RT-PCR tests were used to determine the endogenous expression of CNNMs in HEK-293T cells, which revealed expression of CNNM1, CNNM2, CNNM3, and CNNM4 isoforms (Fig.13.F). We used CRISPR/Cas9 in collaboration with Dr. Zhiyong Bai, a postdoctoral fellow in the Runnels laboratory, to knockout CNNM3 and CNNM4, individual and altogether in 293-TRPM7 cells (293-M7-ΔCNNM3, 293-M7-ΔCNNM4, 293-M7-ΔCNNM3/4) (Fig.13a,b). For each individual cell knockout line, three separate clones were produced, and Dr. Bai used SDS-PAGE and Western blotting to confirm the loss of CNNM isoforms in these cell lines (Fig.2c). Dr. Bai and I worked together to demonstrate that knockout out CNNMs had little effect on TRPM7 protein levels (Fig.13d). We further did cell surface biotinylation experiments to demonstrate that knockout of CNNM3 and CNNM4 does not affect the channel's expression on the cell surface (Fig.13e). Dr. Bai conducted functional studies using a Zn^{2+}-influx assay to measure TRPM7 channel function, which relies on the fact that TRPM7 is most permeable to Zn^{2+} cations. Ten micromolar $ZnCl_2$ is added to the extracellular buffer and the resulting Zn^{2+} influx through the channel causes intracellular Zn^{2+} to rise, which can be detected using fluorescent Zn^{2+} indicator Fluo-Zin-3 (see Material and Methods). The Zn^{2+}-influx assay was employed to demonstrate that knockout of CNNM3 from 293-TRPM7 cell decreased Zn^{2+} influx by approximately half as compared to the 293-TRPM7 parental cell line, while knockout of CNNM4 induced a more significant reduction in TRPM7-dependent Zn^{2+} influx (Fig.13a,b). The combined knockout of CNNM3 and CNNM4 did not lower TRPM7-dependent Zn^{2+} influx below that seen in 293-M7-CNNM4 cells (Fig.13a). These results

indicates that although CNNM3 contributes to TRPM7-mediated Zn^{2+} influx, native CNNM4 appears to be the more potent TRPM7 channel regulator. Dr. Bai performed gain-of-function tests to see whether re-expression of CNNM3, CNNM4, or CNNM3 and CNNM4 together could restore Zn^{2+}-influx (Fig. 13a,b). CNNM3 reexpression in 293-M7-ΔCNNM3 cells increased TRPM7-dependent Zn^{2+} influx to levels comparable to control 293-M7 cells. Re-expression of CNNM4 in 293-M7-ΔCNNM4 cells, on the other hand, increased TRPM7-dependent Zn^{2+} influx beyond that of control 293-M7 cells. Re-expression of CNNM3 in 293-M7-ΔCNNM3/4 cells did not fully restore TRPM7-dependent Zn^{2+} influx to that of control 293-M7 cells, whereas expression of CNNM4 alone in 293-M7-ΔCNNM3/4 cells increased TRPM7-dependent Zn^{2+} influx above that of 293-M7 cells. In 293-M7-CNNM3/4 cells, co-expression of CNNM3 and CNNM4 resulted in the largest rise in Zn^{2+} uptake (Fig.13a,b). Taken together, these results show that both CNNM3 and CNNM4 isoforms play a role in regulating TRPM7 function in 293-TRPM7 cells.

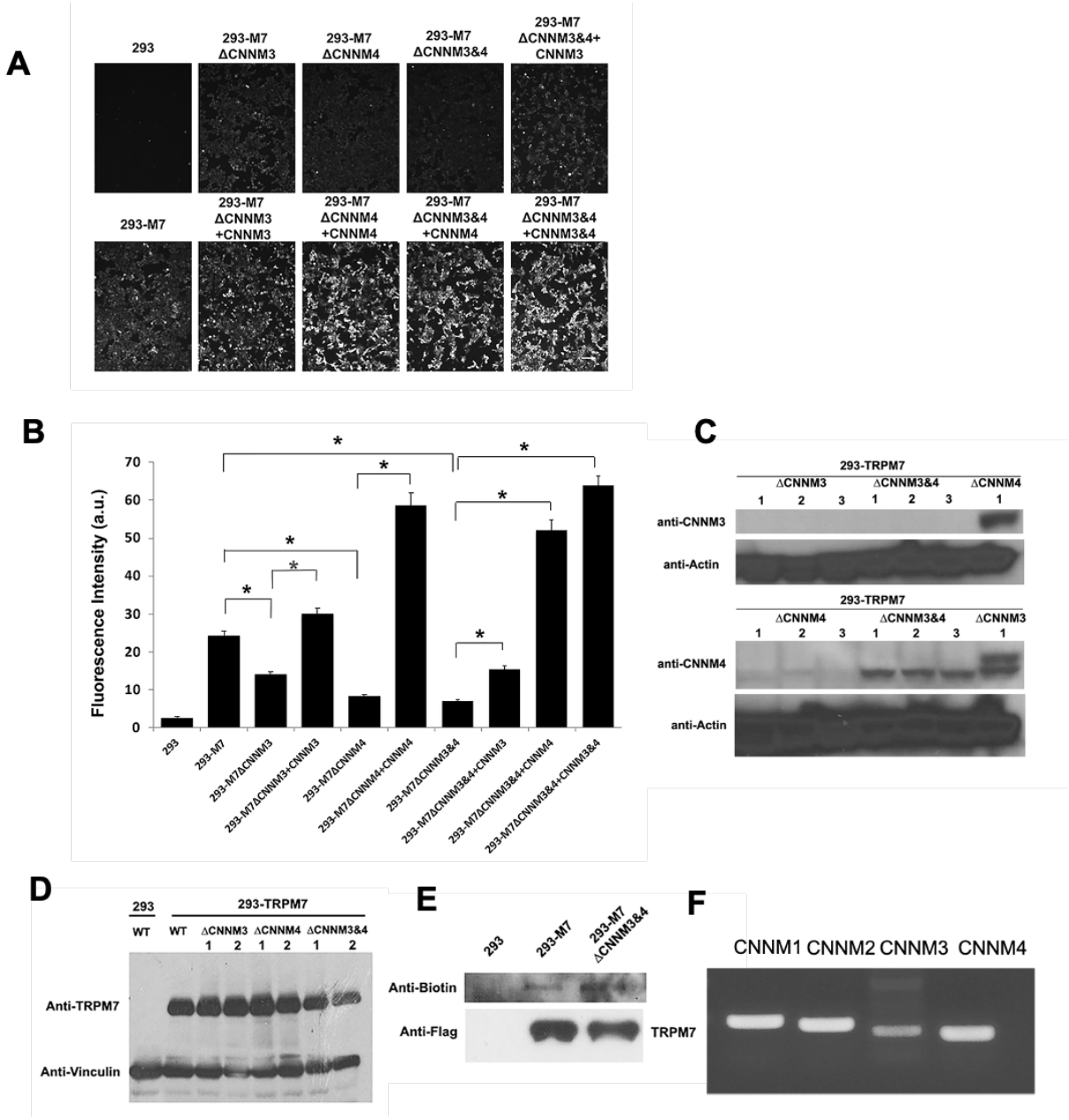

Fig 13. CNNMs are required for TRPM7-mediated Zn^{2+}-influx.

(A) Zinc-influx assay using Fluo-Zin-3 Zn^{2+} indicator was used to monitor TRPM7 function in intact cells. Knockout of *CNNM3*, *CNNM4*, and both *CNNM3* and *CNNM4* from 293-M7 cells (293-M7-ΔCNNM3 293-M7-ΔCNNM4, 293-M7-

ΔCNNM3/4) reduced TRPM7 channel function, which could be rescued to varying degrees by re-expression of CNNM3 and/or CNNM4. All the cells in the assay were treated with tetracycline to induce TRPM7 expression. White scale bar = 100 μm. (B) Quantification of the results from (A). 100 cells were randomly selected for quantification. n=100. * indicates a p value of less than 0.05. (C) CRISPR-Cas9 was used to knockout *CNNM3*, *CNNM4*, and both *CNNM3&4* from 293-TRPM7 cells, which express TRPM7. Western blotting of 3 independent clones showed specific knockout of CNNM isoforms. Two independent clones from each 293-M7 line were also analyzed to demonstrate similar expression of TRPM7 among the lines. (D) Western blot of TRPM7 expression demonstrates similar TRPM7 expression under the +tetracycline conditions in (A). (E) Cell-surface biotinylation of 293-TRPM7 WT and 293-M7-ΔCNNM3/4 cells demonstrate that surface level of TRPM7 in the two cell lines is similar. (F) Agarose gel electrophoresis of RT-PCR amplified products of CNNM1, CNNM2, CNMM3 and CNNM4 from HEK-293T cells.

4.2. CNNMs' Effect on TRPM7 Channel Activity.

In collaboration with Dr. Lixia Yue, we used an electrophysiological approach to more specifically examine the effect of CNNMs on TRPM7 channel activity. When TRPM7 is expressed in WT HEK-293 cells, Dr. Yue's lab discovered that whole-cell recordings of TRPM7 generate whole-cell currents with a large outward current and a distinctive weak inward current (4, 52). To see how CNNMs influence TRPM7 conductance, we used an intracellular solution without Mg^{2+} or Mg-ATP to calculate

current amplitudes in 293-TRPM7 and 293-M7-ΔCNNM3/4 cells with and without re-expression of CNNM4. CNNM4 expression was accomplished with the help of a new cumate-inducible expression vector that I designed and created. TRPM7's current-voltage relationship remained unchanged under these circumstances, but TRPM7 whole-cell currents were greatly decreased in 293-M7-ΔCNNM3/4 cells relative to parental 293-TRPM7 cells (Fig.14a). The recorded TRPM7 currents increased when CNNM4 was re-expressed in 293-M7-ΔCNNM3/4 cells. TRPM7 behavior is severely reduced in the absence of CNNMs, which is compatible with the diminished Zn^{2+} influx (Fig. 13a,b) reported in 293-M7-ΔCNNM3/4 cells. Our findings indicate that CNNMs are necessary for TRPM7 channel function and that the CNNM-TRPM7 complex represents a novel divalent cation influx pathway.

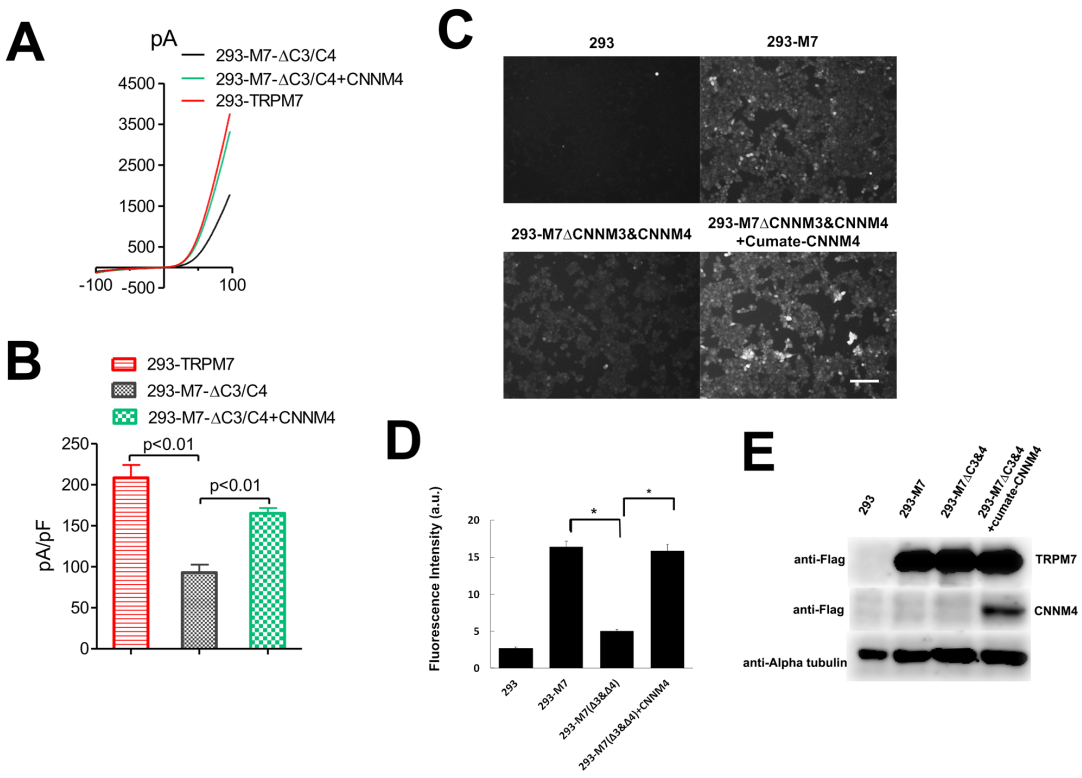

Figure 14. Functional assessment of CNNMs on TRPM7 channel activity.

TRPM7 currents were recorded in 293-TRPM7 cells (n=30), 293-M7-ΔCNNM3/4 cells (n=30), and 293-M7-ΔCNNM3/4 cells (n=40) with stable episomal expression of CNNM4 to keep CNNM4 protein levels low. (A) Representative TRPM7 whole-cell currents from the three cell lines recorded with an internal pipette solution containing 0 Mg^{2+}/Mg-ATP to achieve full TRPM7 channel activity. (B) Average current density of the different groups from (A). (C) Zinc-influx assay using Fluo-Zin-3 Zn^{2+} indicator was used to monitor TRPM7 function in cells from (a). White scale bar = 100 μM. (D) Quantification of results from (C). 100 cells were randomly selected for quantification. n=100. * indicates a p value of less than 0.05. (E)

Western blot demonstrating CNNM4 expression in the cell groups used in (A & C).

SECTION 5. TRPM7 Regulation by ARL15.

5.1 Interaction of TRPM7 with ARL15 and its Effect on Channel Expression.

ARL15 was found to be a potential interacting protein of TRPM7, according to our mass spectrometery study. To confirm this result, we conducted co-immunoprecipitation experiments to determine whether ARL15 interacts with TRPM7. Our results show that TRPM7 does not co-immunoprecipiate (Figure 15). The reason for this is not clear. One possibility is that ARL15 binds to CNNMs and therefore CNNMs are required for TRPM7 and ARL15 to associate. This will be tested in future studies. Nevertheless, a functional interaction between TRPM7 and ARL15 was detected. Dr. Bai next conducted a Zn^{2+}-influx experiment to evaluate the impact of ARL15 on TRPM7 function. His experiments revealed a decrease in TRPM7 channel function when HEK-293 cells are made to overexpress (Figure 16A). ARL15. If overexpression of ARL15 reduces Zn^{2+} Influx in TRPM7-expressing cells, would knockdown of ARL15 in 293-TRPM7 produce the opposite results? We used siRNA technology (ARL15 siRNA1, ARL15 siRNA2) to knockdown ARL15 in TRPM7-stably expressed cells and evaluated the knockdown in ARL15 protein expression by Western blotting (Figure 16C). We next tested the effect of transfection of siRNAs targeting ARL15 on Zn^{2+}-influx stimulated by overexpression of TRPM7. Knockdown of ARL15 using the ARL15 siRNA1 and ARL15siRNA2 increased Zn^{2+}-influx in TRPM7 expressing cells

compared to cells transfected with a control siRNA. This data suggests that ARL15 affects TRPM7 function in HEK2-293 cells.

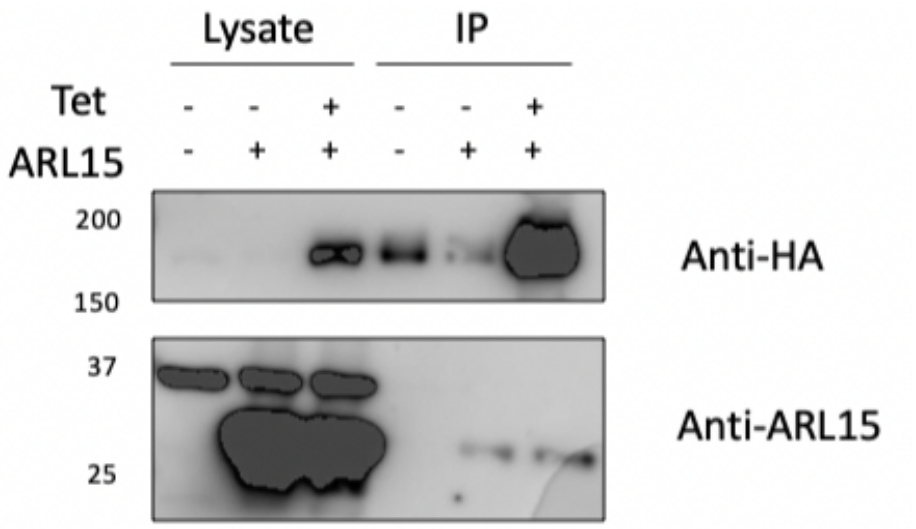

Figure 15. ARL15 does not directly interact with TRPM7

To evaluate whether TRPM7 and ARL15 interact, ARL15 was transiently transfected into 293-TRPM7 cells, which express HA-tagged TRPM7 in the presence of tetracycline (Tet). TRPM7 was effectively immunoprecipitated as detected using the Anti-HA antibody, however, ARL15 failed to effectively co-immunoprecipitate with TRPM7.

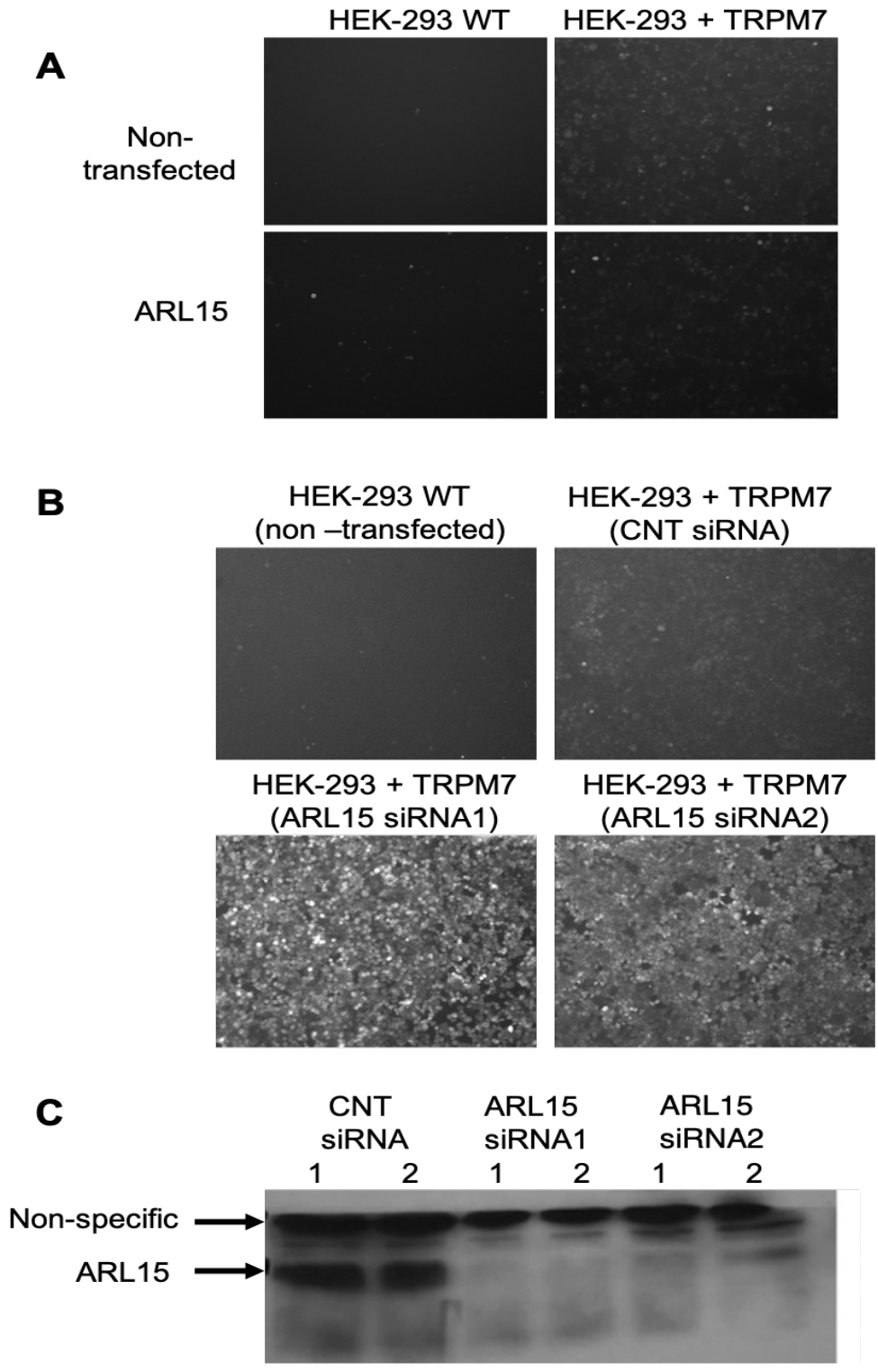

Figure 16. Effect of overexpression and knockdown of ARL15 on TRPM7 function

Zinc-influx assay using Fluo-Zin-3 Zn^{2+} indicator was used to monitor TRPM7

function in intact cells. (A) To test the effect of ARL15 on TRPM7 function, ARL15 was transfected into HEK-293 cells. Co-expression of ARL15 with TRPM7 reduced Zn^{2+}-influx compared to cells only expressing TRPM7. (B). A loss-of-function approach was used to verify the requirement of ARL15 for TRPM7. Knockdown of ARL15 was achieved using siRNAs targeting ARL15 (ARL15 siRNA1 or ARL15siRNA2). The Zinc-influx assay demonstrated that knockdown of ARL15 increases TRPM7 function. (C) Western blot demonstrating that ARL15 siRNA1 and ARL15siRNA2 effectively reduce ARL15 expression compared to a control siRNA (CNT siRNA).

5.2 TRPM7 Localization to the Cell Boundary is Disrupted by ARL15.

ARL15 belongs to the ARF family of small GTPases. It localizes to the cell boundary as expressed in opossum kidney cells proximal tubule epithelial cells. As seen in the immunocytochemistry assay in Figure 17, co-expression of ARL15 with TRPM7 in OK cells interferes with TRPM7 localization to the cell boundary. To understand whether the change in expression at the cell surface was related to an effect of ARL15 on TRPM7 protein expression, we transiently transfected increasing amount of ARL15 or GFP cDNA into 293-TRPM7 cells, which express TRPM7 in the presence of tetracycline (Tet). Western blotting was used to analyze TRPM7 expression after transfection with various amounts of ARL15 cDNA, using GFP cDNA as a negative control. Since GFP should not interfere with TRPM7 expression, we used it as a negative control. Our experiments demonstrate that ARL15 does not significantly affect TRPM7 protein expression, suggesting that ARL15 interferes with TRPM7 function by mostly likely affecting trafficking of the channel.

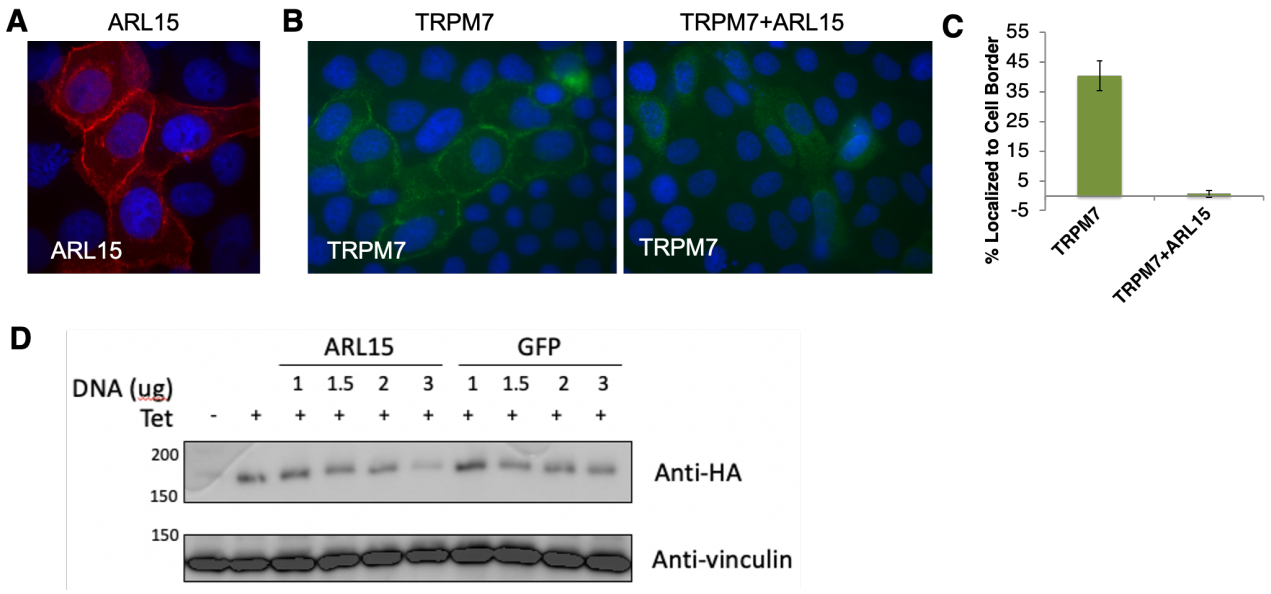

Figure 17. ARL15 disrupts localization of TRPM7 to the cell border.

(A) ARL15 is a small GTPase member of the ARF family. When expressed in OK proximal tubule epithelial cells it localizes to the cell border. (B) Co-expression of ARL15 with TRPM7 in OK cells interferes with TRPM7 localization to the cell border. (C) Quantitation of the results from (B) (n=3). (D). To test whether ARL15 interferes with TRPM7 expression, different amounts of ARL15 or GFP cDNA was transfected into 293-TRPM7 cells expressing HA-tagged TRPM7. Expression of ARL15 did not have a significant effect on TRPM7 protein expression, indicating that the major effect of TRPM7 appears to be on its localization to the cell surface.

DISCUSSION

The goal of this work was to study the role of Mg^{2+} in cytoskeleton regulation and how it plays a role as a second messenger. The previous studies by Scharenberg's group revealed that deletion of TRPM7 in the chicken DT40 B cell line caused cell death after few days in culture[2]. Interestingly, supplementation of the growth media with high magnesium or overexpression of the magnesium transporter (SLC41A2) restored cell survival and proliferation[67, 68]. In addition, TRPM7 has implicated in cytoskeleton regulation. In a previous study by the Runnels' group it was shown that stable knockdown of TRPM7 in Swiss 3T3 fibroblasts caused a disruption in cell morphology, migration and polarization, which are changes all driven by changes to the cytoskeleton[25]. Consistent with the Scharenberg study, overexpression of magnesium transporter (SLC41A2) in TRPM7-knockdown 3T3 fibroblasts rescued the defect that caused by TRPM7 knockdown, suggesting a role for magnesium in TRPM7 function[25]. When magnesium levels in TRPM7 knockdown cells were analyzed, it was found that it was significantly lower than in WT cells; thus, it was concluded that the overexpression of the SLC41A2 corrected the defect in the cytoskeleton by increasing the Mg^{2+} level. Several studies have reported that the Mg^{2+} influences cellular ROS production[69]. Therefore, we hypothesized that the TRPM7 channels may regulate cytoskeleton through influx of Mg^{2+} and subsequently ROS production. Thus, in our current study we proposed that magnesium exerts its effects on cytoskeleton through changes in ROS levels. Our first results, as shown in Figure 4, demonstrate that increasing ROS levels in TRPM7 knockdown cells

by overexpression of the NOX1 enzyme complex corrects the defect in cell morphology cause by knockdown of the TRPM7 channel, with NOX1-expressing cells becoming more spread than the very narrow and long TRPM7 knockdown cells. To confirm the role of ROS in cell morphology regulation, we used another other tool to manipulate ROS levels. Overexpression of catalase, which lowers ROS levels by breaking down hydrogen peroxide into oxygen and water, is one way to lower ROS in the cells. As shown in Fig 6, we found that overexpression of catalase (CAT1) lowered cellular ROS levels, which then led to defect in cell morphology similar to what we observed when TRPM7 is knocked down in Swiss 3T3 cells. Until recently, the generation of reactive oxygen species (ROS) in cells was considered undesired and a negative byproduct of oxidative respiration. Now ROS are also considered as signaling molecules and have been found to be involved in the regulation of many cellular functions, including cell proliferation, cell migration, cell adhesion and cytoskeleton regulation [35, 70-72]. For example, evidence from one study showed that Nox1 has important role in endothelial cell migration during angiogenesis and that depletion of Nox1 interfered with cell migration of these cells (55). Similarly, an *in vivo* study with Nox1 deficient mice revealed a reduction in PDGF-induced cell migration; conversely, Nox1 transgenic mice exhibited an increase in PDGF-induced cell migration (61). Consistent with our result that showed overexpression of catalase (Fig 6) produces a defect in cell morphology in 3T3 fibroblasts, a study reported that phenylephrine and VSMF induced migration are prevented by catalase treatment and application of the antioxidant N-acetyl-cysteine (NAC) [73, 74]. In addition, a study by Chiarugi and

coworkers revealed that treating the NIH 3T3 cells with 5 μM NDGA or 10 μM DPI and NAC inhibits cells adhesion and cell spreading. Therefore, ROS clearly has an impact on cell migration. The questions for us were whether there was a connection between changes in intracellular Mg^{2+} and changes in ROS levels caused by depletion of TRPM7 in cells.

In earlier experiments by the Runnels group, changes in intracellular magnesium were shown to have specific effects on cell morphology and the cytoskeleton. Our lab identified TRPM7 as the main entry for Mg^{2+} in Swiss 3T3 fibroblast cells because it was observed that knockdown of TRPM7 in these cells prevented an increase in intracellular Mg^{2+} that normally occurs when Mg^{2+} is supplemented to the growth media. In addition, overexpression of the Mg^{+2} transporter SLC41A2 (Fig 4) rescued the defect caused by TRPM7 knockdown. In our present study we showed that lowering Mg^{2+} levels in 3T3 cells, independent of manipulation of TRPM7 levels, through overexpression of CNMM2 (Fig 8) caused a change in cell morphology similar to what occurs in TRPM7 knockdown cells, with CNNM2-overexpressing cell morphology becoming thinner and longer. Thus, it is the change in intracellular Mg^{2+} that is critical to the control of cell morphology and the cytoskeleton. One explanation for this observation stems from the fact that Mg^{2+} regulates many enzymes that control many cellular functions. In addition, Mg^{2+} is a cofactor for many enzyme's activity. Accordingly, lowering the Mg^{2+} in fibroblast could directly affect the enzymes that regulate cytoskeleton. Rather, our experiments show that it is the profound change in ROS levels that appears to be central to Mg^{2+}'s effect on cell morphology and the cytoskeleton.

How does a change in intracellular Mg^{2+} affect cellular ROS levels? One possibility is that Mg^{2+} affects an enzyme that is involved in ROS generation and that lowering of Mg^{2+} lowers ROS production to cause the change in cell morphology and the cytoskeleton. A big reservoir of Mg^{2+} inside the cell is the mitochondria and the mitochondria is involved in ROS production. It has been shown that the production of ROS by mitochondria is Mg^{2+} dependent[75]. Future work will focus on whether Mg^{2+}-dependent changes in intracellular ROS production by mitochondria is what is responsible for Mg^{2+} influence on cell morphology and the cytoskeleton. In addition, the mechanism by which Mg^{2+}-dependent changes in intracellular ROS influence the cytoskeleton needs to be further defined.

Thus, one important question we attempted to address was by which mechanism(s) does ROS effect on the cytoskeleton. The first candidate we chose to explore was Focal Adhesion kinase (FAK), which has a central role in integrin signaling and cells movement [76]. In addition to its association with integrin-mediated cell adhesion complexes, FAK kinase is also localized at intercellular junctions, like adherence junctions [77]. Chiarugi and coworker demonstrated that the generation of ROS are necessary for integrin signaling during cell adhesion and cell spreading in NIH 3T3 cells. The authors reported that ROS levels rose ten-fold following integrin engagement, which produced changes in cell adhesion and cytoskeleton organization [38]. Based on this previous study we thought that FAK would be a good candidate for mediating the changes in cell morphology and cytoskeleton that occur through manipulation of Mg^{2+} levels. However, our

experiments failed to detect any changes in FAK activation in response to overexpression of CNNM2 or catalase (Fig3,5) indicating that FAK is not the primary mechanisms by which Mg^{2+} exerts its influence on the cytoskeleton, indicating that other molecules besides FAK are involved.

c-Src was another possible candidate we explored as a mediator of Mg^{2+}-dependent changes in the cytoskeleton. c-Src kinase activity also has been shown to be involved in the activity of FAK in different cells [78]. In the study of the Shyamali Basuroy and colleagues, oxidative stress was shown to induce the activity of c-Src and subsequently activate FAK and phosphorylation at Y397, Y925 and Y577. The FAK phosphorylation vents enhanced the Caco-2 cells migration [79]. Therefore, we speculated that Mg^{2+}-dependent changes in ROS levels could be exerting its effects on cell morphology through inhibition of the activity of Src kinase. We investigated the impact of lowering ROS and Mg^{2+} in Swiss 3T3 fibroblasts on the activation of Src kinases by overexpression of CAT1 and CNNM2 in the cells, respectively. We found that overexpression of either CAT1 or CNNM2 did not disrupt Src kinase activation (Fig 12). Thus, it still remains unclear how Mg^{2+}-dependent changes in ROS affects cell morphology and the cytoskeleton. ROS has many other target proteins that are potentially involved in cytoskeleton regulation. Therefore, future work will need to address the mechanisms by which Mg^{2+} and ROS exerts its effects on cell morphology and the cytoskeleton.

Finally, we reported collaborative work we performed with Dr. Zhiyong Bai in his investigation of the role of CNNM and ARL15 proteins in regulating TRPM7. Our

efforts demonstrated that CNNM proteins are required for TRPM7 activity in HEK-293 cells, as assessed using a Zn^{2+}-influx assay and electrophysiology. This discovery in an important advance which will give significant insight into how the channel is regulated *in vivo*. We also conducted experiments on ARL15 effect on TRPM7 function. Our studies indicated that ARL15 does not appear to directly interact with TRPM7. Future work will focus on whether CNNM proteins are required for ARL15 and TRPM7 to associate *in vivo*. Nevertheless, our experiments revealed that ARL15 is a potent regulator of TRPM7 function. Overexpression of ARL15 decreased TRPM7 channel function in HEK-293 cells, as assessed using a Zn^{2+}-influx assay. Conversely, knockdown of ARL15 using two independent siRNAs increased TRPM7 channel function. This data indicates that ARL15 is a negative regulation of the channel. We conducted experiments to elucidate the mechanism by which ARL15 affects TRPM7 and discovered that overexpression of ARL15 in OK cells decreases the amount of the channel localized to the cell border. Apparently, the decrease is not due to a decrease in TRPM7 protein expression as overexpression of ARL15 had no effect on channel protein expression. Together these results suggest that ARL15 affects trafficking of the channel either to or from the cell surface. Future studies will investigate this hypothesis. Nevertheless, this collective work has revealed CNNM and ARL15 proteins as novel regulators of the TRPM7 channel.

FUTURE DIRECTIONS

There are two areas of investigation that we could pursue to better understand how Mg^{2+}-dependent changes in ROS affects the cytoskeleton. First, it would be important to identify the source(s) of Mg^{2+}-dependent ROS generation. Second, as discussed above, the molecular target of ROS still remains unknown. Our experiments have uncovered an experimental approach that could be explored to address this question. One could use TRPM7-knockdown cells and overexpress the Mg^{2+} transporter SLC41A2 and assess whether application of chemical inhibitors of sources of ROS production block the rescue in cell morphology from a spindle shape to a spread cell shape. The main sources of ROS in cells are from the NADPH oxidases (NOX), lipoxygenases (LOXs), and as discussed earlier, the respiratory chain of mitochondria. One could use the inhibitor diphenyl-iodide (DPI) to block NADPH oxidase, nordihydroguaiaretic acid (NDGA) to block LOX, and the chemical rotenone to inhibit the mitochondrial superoxide production. By examining the extent by which these chemical inhibitors affect SLC41A2-dependent changes in cell morphology and changes in cell morphology one could tease apart which source of ROS is responsible for Mg^{2+}-dependent control of the cytoskeleton.

To address the question of what the molecular target of ROS is in cells, one could employ a proteomic approach using mass spectrometry to identify residues in proteins that are oxidized in response to overexpression of SLC41A2 in TRPM7-knockdown cells. One good tool to detect redox modification is the BIAM (biotinylated iodoacetamide) switch assay, which is a biotin-based tagging

technique has been used to detect the intracellular thiol status of protein after exposure to ROS. Briefly, this approach involves 3 steps which are: 1) Blocking of the reduced thiols. 2) Reducing and labelling with BIAM. 3) Enrichment of BIAM-labeled protein with streptavidin beads and then subjecting the samples to Western bolt or mass spectrometry. Using this method, we can compare the redox modification between the TRPM7 knockdown stable cells line and overexpression of SLC41A2 in TRPM7-knockdown cells, since SLC41A2 increase intracellular level of Mg^{2+} and ROS in these cells.

CONCLUSION

In conclusion, our observations in this project indicate that Mg^{2+} per se has important role in the regulation the cytoskeleton in Swiss 3T3 fibroblasts. A dramatic change in cell morphology and the cytoskeleton can be produced either by targeted knockdown of TRPM7 in fibroblasts or by the lowering of Mg^{2+} by overexpression of CNNM2 in cells. We also observed that we can correct the cell morphology and cytoskeleton defects caused by TRPM7 knockdown by increasing intracellular ROS levels, indicating that Mg^{2+} regulates the cell morphology through ROS, which subsequently affects other as of now unknown downstream target molecules that regulate the cytoskeleton (Figure 18). Although more research is needed to elucidate how Mg^{2+} controls the generation of ROS and to identify the molecules that ROS is targeting, we can conclude that ROS is a major effector of Mg^{2+} in the control of cell morphology and the actin cytoskeleton.

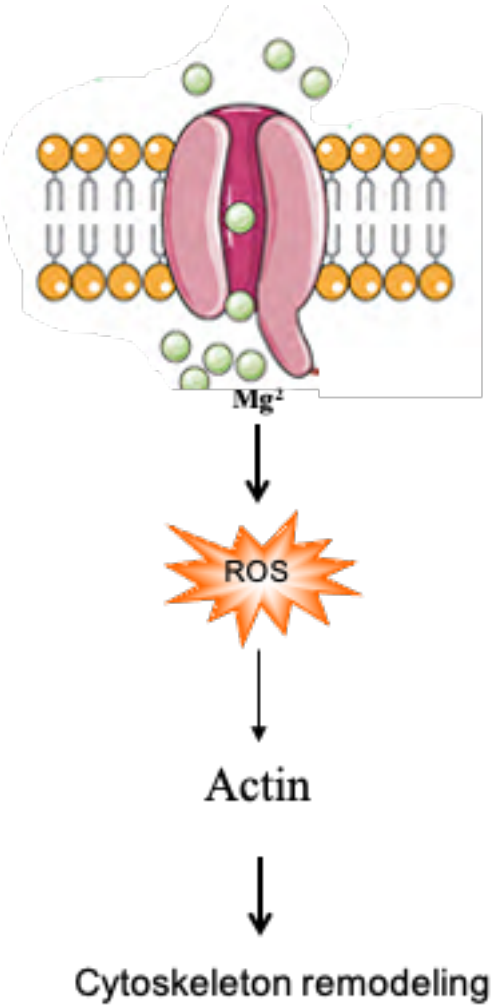

Figure 18: Working Model for how Mg^{2+} Regulates Cell Migration by Controlling ROS levels.

Our hypothesis is that magnesium conducted through the TRPM7 channel regulates the cytoskeleton in Swiss 3T3 fibroblast by changing the levels of intracellular ROS, which has many potential molecular, including actin, as was identified in our study.

ABBREVIATIONS

ATCC, American Type Culture Collection

BIAM, biotinylated iodoacetamide

CAT, Catalase

D-MEM, Dulbecco's Modified Eagle Medium

DAPI, 4',6-diamidino-2-phenylindole

DMSO, dimethyl sulfoxide

DPI, diphenyl-iodide

FBS, fetal bovine serum

H2DCFDA, dichlorodihydrofluorescein diacetate

HEK, human embryonic kidney

HMEC, human human microvascular endothelial cells (HMEC)

NAC, N-acetylcysteine

NDGA, nordihydroguaiaretic acid

Nox1, NADPH oxidase

PBS, phosphate buffered saline

PCR, polymerase chain reaction

PDGF, Platelet drive growth factor

ROS, Reactive oxygen species.

SDS-PAGE, sodium dodecyl sulfate-polyacrylamide gel electrophoresis

SDS, sodium dodecyl sulfate

TRPM, transient receptor potential melastatin

VSMF, vascular smooth muscle factor

WT, wild type

NOXO1, NADPH oxidase organizer 1

NOXA1, NADPH oxidase activator 1

SLC41A2, Solute Carrier Family 41 Member 2

CNNM2, Cyclin and CBS Domain Divalent Metal Cation Transport Mediator 2.

LacZ, bacterial beta-galactosidase gene

H2O2, Hydrogen peroxide

LOX, lipoxygenases

REFERENCES

1. Runnels LW, Yue L, Clapham DE. TRP-PLIK, a bifunctional protein with kinase and ion channel activities. Science. 2001;291(5506):1043-7. Epub 2001/01/18. doi: 10.1126/science.1058519. PubMed PMID: 11161216.
2. Nadler MJ, Hermosura MC, Inabe K, Perraud AL, Zhu Q, Stokes AJ, Kurosaki T, Kinet JP, Penner R, Scharenberg AM, Fleig A. LTRPC7 is a Mg.ATP-regulated divalent cation channel required for cell viability. Nature. 2001;411(6837):590-5. doi: 10.1038/35079092. PubMed PMID: 11385574.
3. Monteilh-Zoller MK, Hermosura MC, Nadler MJ, Scharenberg AM, Penner R, Fleig A. TRPM7 provides an ion channel mechanism for cellular entry of trace metal ions. J Gen Physiol. 2003;121(1):49-60. doi: 10.1085/jgp.20028740. PubMed PMID: 12508053; PMCID: PMC2217320.
4. Clark K, Langeslag M, van Leeuwen B, Ran L, Ryazanov AG, Figdor CG, Moolenaar WH, Jalink K, van Leeuwen FN. TRPM7, a novel regulator of actomyosin contractility and cell adhesion. EMBO J. 2006;25(2):290-301. Epub 2006/01/12. doi: 10.1038/sj.emboj.7600931. PubMed PMID: 16407977; PMCID: PMC1383514.
5. Visser D, Langeslag M, Kedziora KM, Klarenbeek J, Kamermans A, Horgen FD, Fleig A, van Leeuwen FN, Jalink K. TRPM7 triggers Ca2+ sparks and invadosome formation in neuroblastoma cells. Cell Calcium. 2013;54(6):404-15. Epub 2013/10/16. doi: 10.1016/j.ceca.2013.09.003. PubMed PMID: 24176224; PMCID: PMC4912378.
6. Zhu D, You J, Zhao N, Xu H. Magnesium Regulates Endothelial Barrier Functions through TRPM7, MagT1, and S1P1. Adv Sci (Weinh). 2019;6(18):1901166. doi: 10.1002/advs.201901166. PubMed PMID: 31559137; PMCID: PMC6755513.
7. Jin J, Desai BN, Navarro B, Donovan A, Andrews NC, Clapham DE. Deletion of Trpm7 disrupts embryonic development and thymopoiesis without altering Mg2+ homeostasis. Science. 2008;322(5902):756-60. Epub 2008/11/01. doi: 10.1126/science.1163493. PubMed PMID: 18974357; PMCID: PMC2605283.
8. Ryazanova LV, Rondon LJ, Zierler S, Hu Z, Galli J, Yamaguchi TP, Mazur A, Fleig A, Ryazanov AG. TRPM7 is essential for Mg(2+) homeostasis in mammals. Nat Commun. 2010;1:109. Epub 2010/11/02. doi: 10.1038/ncomms1108. PubMed PMID: 21045827; PMCID: PMC3060619.
9. Liu W, Su LT, Khadka DK, Mezzacappa C, Komiya Y, Sato A, Habas R, Runnels LW. TRPM7 regulates gastrulation during vertebrate embryogenesis. Developmental biology. 2011;350(2):348-57. Epub 2010/12/15. doi: 10.1016/j.ydbio.2010.11.034. PubMed PMID: 21145885.
10. Deason-Towne F, Perraud AL, Schmitz C. The Mg2+ transporter MagT1 partially rescues cell growth and Mg2+ uptake in cells lacking the channel-kinase TRPM7. FEBS Lett. 2011;585(14):2275-8. Epub 2011/05/27. doi: 10.1016/j.febslet.2011.05.052. PubMed PMID: 21627970; PMCID: PMC3139019.
11. Cheng H, Feng JM, Figueiredo ML, Zhang H, Nelson PL, Marigo V, Beck A. Transient receptor potential melastatin type 7 channel is critical for the survival of bone marrow derived mesenchymal stem cells. Stem Cells Dev. 2010;19(9):1393-403. doi: 10.1089/scd.2009.0262. PubMed PMID: 19929312; PMCID: PMC3128316.
12. Komiya Y, Runnels LW. TRPM channels and magnesium in early embryonic development. Int J Dev Biol. 2015;59(7-9):281-8. doi: 10.1387/ijdb.150196lr. PubMed PMID: 26679946; PMCID: PMC4685952.
13. de Baaij JH, Hoenderop JG, Bindels RJ. Magnesium in man: implications for health and disease. Physiological reviews. 2015;95(1):1-46. doi: 10.1152/physrev.00012.2014. PubMed PMID: 25540137.

14. Grubbs RD, Maguire ME. Magnesium as a regulatory cation: criteria and evaluation. Magnesium. 1987;6(3):113-27. PubMed PMID: 3306178.
15. Romani AM. Cellular magnesium homeostasis. Arch Biochem Biophys. 2011;512(1):1-23. doi: 10.1016/j.abb.2011.05.010. PubMed PMID: 21640700; PMCID: PMC3133480.
16. Prescott AR, Comerford JG, Magrath R, Lamb NJ, Warn RM. Effects of elevated intracellular magnesium on cytoskeletal integrity. J Cell Sci. 1988;89 (Pt 3):321-9. PubMed PMID: 3198695.
17. Su LT, Agapito MA, Li M, Simonson WT, Huttenlocher A, Habas R, Yue L, Runnels LW. TRPM7 regulates cell adhesion by controlling the calcium-dependent protease calpain. The Journal of biological chemistry. 2006;281(16):11260-70. Epub 2006/01/27. doi: 10.1074/jbc.M512885200. PubMed PMID: 16436382; PMCID: PMC3225339.
18. Su LT, Chen HC, Gonzalez-Pagan O, Overton JD, Xie J, Yue L, Runnels LW. TRPM7 activates m-calpain by stress-dependent stimulation of p38 MAPK and c-Jun N-terminal kinase. J Mol Biol. 2010;396(4):858-69. Epub 2010/01/15. doi: S0022-2836(10)00030-6 [pii]
10.1016/j.jmb.2010.01.014. PubMed PMID: 20070945; PMCID: 2825087.
19. Abed E, Moreau R. Importance of melastatin-like transient receptor potential 7 and magnesium in the stimulation of osteoblast proliferation and migration by platelet-derived growth factor. American journal of physiology Cell physiology. 2009;297(2):C360-8. Epub 2009/05/29. doi: 10.1152/ajpcell.00614.2008. PubMed PMID: 19474290.
20. Baldoli E, Maier JA. Silencing TRPM7 mimics the effects of magnesium deficiency in human microvascular endothelial cells. Angiogenesis. 2012;15(1):47-57. Epub 2011/12/21. doi: 10.1007/s10456-011-9242-0. PubMed PMID: 22183257.
21. Chen L, Cao R, Wang G, Yuan L, Qian G, Guo Z, Wu CL, Wang X, Xiao Y. Downregulation of TRPM7 suppressed migration and invasion by regulating epithelial-mesenchymal transition in prostate cancer cells. Medical oncology (Northwood, London, England). 2017;34(7):127. Epub 2017/06/03. doi: 10.1007/s12032-017-0987-1. PubMed PMID: 28573641.
22. Cui L, Xu SM, Ma DD, Wu BL. The effect of TRPM7 suppression on the proliferation, migration and osteogenic differentiation of human dental pulp stem cells. International endodontic journal. 2014;47(6):583-93. Epub 2013/10/22. doi: 10.1111/iej.12193. PubMed PMID: 24138320.
23. Leng TD, Li MH, Shen JF, Liu ML, Li XB, Sun HW, Branigan D, Zeng Z, Si HF, Li J, Chen J, Xiong ZG. Suppression of TRPM7 inhibits proliferation, migration, and invasion of malignant human glioma cells. CNS neuroscience & therapeutics. 2015;21(3):252-61. Epub 2014/12/03. doi: 10.1111/cns.12354. PubMed PMID: 25438992; PMCID: PMC4339490.
24. Middelbeek J, Kuipers AJ, Henneman L, Visser D, Eidhof I, van Horssen R, Wieringa B, Canisius SV, Zwart W, Wessels LF, Sweep FC, Bult P, Span PN, van Leeuwen FN, Jalink K. TRPM7 is required for breast tumor cell metastasis. Cancer research. 2012;72(16):4250-61. Epub 2012/08/09. doi: 10.1158/0008-5472.can-11-3863. PubMed PMID: 22871386.
25. Su LT, Liu W, Chen HC, Gonzalez-Pagan O, Habas R, Runnels LW. TRPM7 regulates polarized cell movements. The Biochemical journal. 2011;434(3):513-21. Epub 2011/01/07. doi: 10.1042/bj20101678. PubMed PMID: 21208190; PMCID: PMC3507444.
26. Wong R, Turlova E, Feng ZP, Rutka JT, Sun HS. Activation of TRPM7 by naltriben enhances migration and invasion of glioblastoma cells. Oncotarget. 2017;8(7):11239-48. Epub 2017/01/07. doi: 10.18632/oncotarget.14496. PubMed PMID: 28061441; PMCID: PMC5355261.
27. Stritt S, Nurden P, Favier R, Favier M, Ferioli S, Gotru SK, van Eeuwijk JM, Schulze

H, Nurden AT, Lambert MP, Turro E, Burger-Stritt S, Matsushita M, Mittermeier L, Ballerini P, Zierler S, Laffan MA, Chubanov V, Gudermann T, Nieswandt B, Braun A. Defects in TRPM7 channel function deregulate thrombopoiesis through altered cellular Mg(2+) homeostasis and cytoskeletal architecture. Nature communications. 2016;7:11097. Epub 2016/03/30. doi: 10.1038/ncomms11097. PubMed PMID: 27020697; PMCID: PMC4820538.
28. Walder RY, Yang B, Stokes JB, Kirby PA, Cao X, Shi P, Searby CC, Husted RF, Sheffield VC. Mice defective in Trpm6 show embryonic mortality and neural tube defects. Hum Mol Genet. 2009;18(22):4367-75. doi: 10.1093/hmg/ddp392. PubMed PMID: 19692351; PMCID: PMC2766295.
29. Schlingmann KP, Weber S, Peters M, Niemann Nejsum L, Vitzthum H, Klingel K, Kratz M, Haddad E, Ristoff E, Dinour D, Syrrou M, Nielsen S, Sassen M, Waldegger S, Seyberth HW, Konrad M. Hypomagnesemia with secondary hypocalcemia is caused by mutations in TRPM6, a new member of the TRPM gene family. Nature genetics. 2002;31(2):166-70. doi: 10.1038/ng889. PubMed PMID: 12032568.
30. Walder RY, Landau D, Meyer P, Shalev H, Tsolia M, Borochowitz Z, Boettger MB, Beck GE, Englehardt RK, Carmi R, Sheffield VC. Mutation of TRPM6 causes familial hypomagnesemia with secondary hypocalcemia. Nature genetics. 2002;31(2):171-4. doi: 10.1038/ng901. PubMed PMID: 12032570.
31. Komiya Y, Bai Z, Cai N, Lou L, Al-Saadi N, Mezzacappa C, Habas R, Runnels LW. A Nonredundant Role for the TRPM6 Channel in Neural Tube Closure. Sci Rep. 2017;7(1):15623. doi: 10.1038/s41598-017-15855-y. PubMed PMID: 29142255; PMCID: PMC5688082.
32. Chen HC, Su LT, Gonzalez-Pagan O, Overton JD, Runnels LW. A Key Role for Mg2+ in TRPM7's Control of ROS Levels During Cell Stress. The Biochemical journal. 2012. Epub 2012/05/17. doi: 10.1042/BJ20120248. PubMed PMID: 22587440.
33. Cross CE, Halliwell B, Borish ET, Pryor WA, Ames BN, Saul RL, McCord JM, Harman D. Oxygen radicals and human disease. Ann Intern Med. 1987;107(4):526-45. doi: 10.7326/0003-4819-107-4-526. PubMed PMID: 3307585.
34. Finkel T. Signal transduction by reactive oxygen species. J Cell Biol. 2011;194(1):7-15. doi: 10.1083/jcb.201102095. PubMed PMID: 21746850; PMCID: PMC3135394.
35. Brown DI, Griendling KK. Regulation of signal transduction by reactive oxygen species in the cardiovascular system. Circ Res. 2015;116(3):531-49. doi: 10.1161/CIRCRESAHA.116.303584. PubMed PMID: 25634975; PMCID: PMC4392388.
36. Shadel GS, Horvath TL. Mitochondrial ROS signaling in organismal homeostasis. Cell. 2015;163(3):560-9. doi: 10.1016/j.cell.2015.10.001. PubMed PMID: 26496603; PMCID: PMC4634671.
37. Brown DI, Griendling KK. Nox proteins in signal transduction. Free Radic Biol Med. 2009;47(9):1239-53. doi: 10.1016/j.freeradbiomed.2009.07.023. PubMed PMID: 19628035; PMCID: PMC2763943.
38. Chiarugi P, Pani G, Giannoni E, Taddei L, Colavitti R, Raugei G, Symons M, Borrello S, Galeotti T, Ramponi G. Reactive oxygen species as essential mediators of cell adhesion: the oxidative inhibition of a FAK tyrosine phosphatase is required for cell adhesion. J Cell Biol. 2003;161(5):933-44. doi: 10.1083/jcb.200211118. PubMed PMID: 12796479; PMCID: PMC2172955.
39. Fiaschi T, Cozzi G, Chiarugi P. Redox Regulation of Nonmuscle Myosin Heavy Chain during Integrin Engagement. J Signal Transduct. 2012;2012:754964. doi: 10.1155/2012/754964. PubMed PMID: 22220276; PMCID: PMC3246775.
40. Xu Q, Huff LP, Fujii M, Griendling KK. Redox regulation of the actin cytoskeleton and its role in the vascular system. Free Radic Biol Med. 2017;109:84-107. doi:

10.1016/j.freeradbiomed.2017.03.004. PubMed PMID: 28285002; PMCID: PMC5497502.
41. Wang CY, Shi JD, Yang P, Kumar PG, Li QZ, Run QG, Su YC, Scott HS, Kao KJ, She JX. Molecular cloning and characterization of a novel gene family of four ancient conserved domain proteins (ACDP). Gene. 2003;306:37-44. doi: 10.1016/s0378-1119(02)01210-6. PubMed PMID: 12657465.
42. Wang CY, Yang P, Shi JD, Purohit S, Guo D, An H, Gu JG, Ling J, Dong Z, She JX. Molecular cloning and characterization of the mouse Acdp gene family. BMC Genomics. 2004;5(1):7. Epub 2004/01/15. doi: 10.1186/1471-2164-5-7. PubMed PMID: 14723793; PMCID: PMC340383.
43. Quamme GA. Molecular identification of ancient and modern mammalian magnesium transporters. Am J Physiol Cell Physiol. 2010;298(3):C407-29. Epub 2009/11/25. doi: 10.1152/ajpcell.00124.2009. PubMed PMID: 19940067.
44. Stuiver M, Lainez S, Will C, Terryn S, Günzel D, Debaix H, Sommer K, Kopplin K, Thumfart J, Kampik NB, Querfeld U, Willnow TE, Němec V, Wagner CA, Hoenderop JG, Devuyst O, Knoers NV, Bindels RJ, Meij IC, Müller D. CNNM2, encoding a basolateral protein required for renal Mg2+ handling, is mutated in dominant hypomagnesemia. Am J Hum Genet. 2011;88(3):333-43. doi: 10.1016/j.ajhg.2011.02.005. PubMed PMID: 21397062; PMCID: PMC3059432.
45. Hirata Y, Funato Y, Takano Y, Miki H. Mg2+-dependent interactions of ATP with the cystathionine-beta-synthase (CBS) domains of a magnesium transporter. The Journal of biological chemistry. 2014;289(21):14731-9. doi: 10.1074/jbc.M114.551176. PubMed PMID: 24706765; PMCID: PMC4031528.
46. Corral-Rodríguez M, Stuiver M, Abascal-Palacios G, Diercks T, Oyenarte I, Ereño-Orbea J, de Opakua AI, Blanco FJ, Encinar JA, Spiwok V, Terashima H, Accardi A, Müller D, Martínez-Cruz LA. Nucleotide binding triggers a conformational change of the CBS module of the magnesium transporter CNNM2 from a twisted towards a flat structure. Biochem J. 2014;464(1):23-34. doi: 10.1042/BJ20140409. PubMed PMID: 25184538; PMCID: PMC7318797.
47. Hardy S, Uetani N, Wong N, Kostantin E, Labbé DP, Bégin LR, Mes-Masson A, Miranda-Saavedra D, Tremblay ML. The protein tyrosine phosphatase PRL-2 interacts with the magnesium transporter CNNM3 to promote oncogenesis. Oncogene. 2015;34(8):986-95. Epub 2014/03/17. doi: 10.1038/onc.2014.33. PubMed PMID: 24632616.
48. Kostantin E, Hardy S, Valinsky WC, Kompatscher A, de Baaij JH, Zolotarov Y, Landry M, Uetani N, Martínez-Cruz LA, Hoenderop JG, Shrier A, Tremblay ML. Inhibition of PRL-2·CNNM3 Protein Complex Formation Decreases Breast Cancer Proliferation and Tumor Growth. J Biol Chem. 2016;291(20):10716-25. Epub 2016/03/11. doi: 10.1074/jbc.M115.705863. PubMed PMID: 26969161; PMCID: PMC4865918.
49. Accogli A, Scala M, Calcagno A, Napoli F, Di Iorgi N, Arrigo S, Mancardi MM, Prato G, Pisciotta L, Nagel M, Severino M, Capra V. CNNM2 homozygous mutations cause severe refractory hypomagnesemia, epileptic encephalopathy and brain malformations. Eur J Med Genet. 2019;62(3):198-203. Epub 2018/07/17. doi: 10.1016/j.ejmg.2018.07.014. PubMed PMID: 30026055.
50. Sponder G, Mastrototaro L, Kurth K, Merolle L, Zhang Z, Abdulhanan N, Smorodchenko A, Wolf K, Fleig A, Penner R, Iotti S, Aschenbach JR, Vormann J, Kolisek M. Human CNNM2 is not a Mg(2+) transporter per se. Pflugers Arch. 2016;468(7):1223-40. Epub 2016/04/11. doi: 10.1007/s00424-016-1816-7. PubMed PMID: 27068403.
51. Yamazaki D, Funato Y, Miyata H, Ikawa M, Miki H. Complementary role of CNNM2 in sperm motility and Ca(2+) influx during capacitation. Biochem Biophys Res Commun. 2016;474(3):441-6. Epub 2016/05/02. doi: 10.1016/j.bbrc.2016.05.001. PubMed PMID: 27150626.

52. Funato Y, Yamazaki D, Miki H. Renal function of cyclin M2 Mg2+ transporter maintains blood pressure. J Hypertens. 2017;35(3):585-92. doi: 10.1097/HJH.0000000000001211. PubMed PMID: 28033128.
53. Ohi K. Influences of schizophrenia risk variant rs7914558 at CNNM2 on brain structure. Br J Psychiatry. 2015;206(4):343-4. doi: 10.1192/bjp.206.4.343b. PubMed PMID: 25833874.
54. Rose EJ, Hargreaves A, Morris D, Fahey C, Tropea D, Cummings E, Caltagirone C, Bossù P, Chiapponi C, Piras F, Spalletta G, Gill M, Corvin A, Donohoe G. Effects of a novel schizophrenia risk variant rs7914558 at CNNM2 on brain structure and attributional style. Br J Psychiatry. 2014;204(2):115-21. Epub 2013/12/05. doi: 10.1192/bjp.bp.113.131359. PubMed PMID: 24311551.
55. Yamazaki D, Funato Y, Miura J, Sato S, Toyosawa S, Furutani K, Kurachi Y, Omori Y, Furukawa T, Tsuda T, Kuwabata S, Mizukami S, Kikuchi K, Miki H. Basolateral Mg2+ extrusion via CNNM4 mediates transcellular Mg2+ transport across epithelia: a mouse model. PLoS Genet. 2013;9(12):e1003983. Epub 2013/12/05. doi: 10.1371/journal.pgen.1003983. PubMed PMID: 24339795; PMCID: PMC3854942.
56. Hirata Y, Funato Y, Takano Y, Miki H. Mg2+-dependent interactions of ATP with the cystathionine-β-synthase (CBS) domains of a magnesium transporter. J Biol Chem. 2014;289(21):14731-9. Epub 2014/04/06. doi: 10.1074/jbc.M114.551176. PubMed PMID: 24706765; PMCID: PMC4031528.
57. Funato Y, Yamazaki D, Mizukami S, Du L, Kikuchi K, Miki H. Membrane protein CNNM4-dependent Mg2+ efflux suppresses tumor progression. J Clin Invest. 2014;124(12):5398-410. Epub 2014/10/27. doi: 10.1172/JCI76614. PubMed PMID: 25347473; PMCID: PMC4348944.
58. Corre T, Arjona FJ, Hayward C, Youhanna S, de Baaij JHF, Belge H, Nägele N, Debaix H, Blanchard MG, Traglia M, Harris SE, Ulivi S, Rueedi R, Lamparter D, Macé A, Sala C, Lenarduzzi S, Ponte B, Pruijm M, Ackermann D, Ehret G, Baptista D, Polasek O, Rudan I, Hurd TW, Hastie ND, Vitart V, Waeber G, Kutalik Z, Bergmann S, Vargas-Poussou R, Konrad M, Gasparini P, Deary IJ, Starr JM, Toniolo D, Vollenweider P, Hoenderop JGJ, Bindels RJM, Bochud M, Devuyst O. Genome-Wide Meta-Analysis Unravels Interactions between Magnesium Homeostasis and Metabolic Phenotypes. J Am Soc Nephrol. 2018;29(1):335-48. Epub 2017/11/01. doi: 10.1681/ASN.2017030267. PubMed PMID: 29093028; PMCID: PMC5748908.
59. Inoue K, Branigan D, Xiong ZG. Zinc-induced neurotoxicity mediated by transient receptor potential melastatin 7 channels. J Biol Chem. 2010. Epub 2010/01/06. doi: M109.040485 [pii]
10.1074/jbc.M109.040485. PubMed PMID: 20048154.
60. Schindelin J, Arganda-Carreras I, Frise E, Kaynig V, Longair M, Pietzsch T, Preibisch S, Rueden C, Saalfeld S, Schmid B, Tinevez JY, White DJ, Hartenstein V, Eliceiri K, Tomancak P, Cardona A. Fiji: an open-source platform for biological-image analysis. Nat Methods. 2012;9(7):676-82. doi: 10.1038/nmeth.2019. PubMed PMID: 22743772; PMCID: PMC3855844.
61. Li M, Du J, Jiang J, Ratzan W, Su LT, Runnels LW, Yue L. Molecular determinants of Mg2+ and Ca2+ permeability and pH sensitivity in TRPM6 and TRPM7. J Biol Chem. 2007;282(35):25817-30. doi: 10.1074/jbc.M608972200. PubMed PMID: 17599911; PMCID: PMC3239414.
62. Hurd TR, DeGennaro M, Lehmann R. Redox regulation of cell migration and adhesion. Trends Cell Biol. 2012;22(2):107-15. doi: 10.1016/j.tcb.2011.11.002. PubMed PMID: 22209517; PMCID: PMC4515034.
63. Cheng G, Lambeth JD. NOXO1, regulation of lipid binding, localization, and activation of Nox1 by the Phox homology (PX) domain. The Journal of biological chemistry.

2004;279(6):4737-42. doi: 10.1074/jbc.M305968200. PubMed PMID: 14617635.
64. Bai J, Cederbaum AI. Catalase protects HepG2 cells from apoptosis induced by DNA-damaging agents by accelerating the degradation of p53. The Journal of biological chemistry. 2003;278(7):4660-7. doi: 10.1074/jbc.M206273200. PubMed PMID: 12468545.
65. Bai J, Rodriguez AM, Melendez JA, Cederbaum AI. Overexpression of catalase in cytosolic or mitochondrial compartment protects HepG2 cells against oxidative injury. The Journal of biological chemistry. 1999;274(37):26217-24. doi: 10.1074/jbc.274.37.26217. PubMed PMID: 10473575.
66. Giannoni E, Buricchi F, Raugei G, Ramponi G, Chiarugi P. Intracellular reactive oxygen species activate Src tyrosine kinase during cell adhesion and anchorage-dependent cell growth. Mol Cell Biol. 2005;25(15):6391-403. doi: 10.1128/MCB.25.15.6391-6403.2005. PubMed PMID: 16024778; PMCID: PMC1190365.
67. Schmitz C, Perraud AL, Johnson CO, Inabe K, Smith MK, Penner R, Kurosaki T, Fleig A, Scharenberg AM. Regulation of vertebrate cellular Mg2+ homeostasis by TRPM7. Cell. 2003;114(2):191-200. doi: 10.1016/s0092-8674(03)00556-7. PubMed PMID: 12887921.
68. Sahni J, Nelson B, Scharenberg AM. SLC41A2 encodes a plasma-membrane Mg2+ transporter. Biochem J. 2007;401(2):505-13. doi: 10.1042/BJ20060673. PubMed PMID: 16984228; PMCID: PMC1820800.
69. Yamaguchi T, Kaneda M, Kakinuma K. Essential requirement of magnesium ion for optimal activity of the NADPH oxidase of guinea pig polymorphonuclear leukocytes. Biochem Biophys Res Commun. 1983;115(1):261-7. doi: 10.1016/0006-291x(83)90998-1. PubMed PMID: 6311205.
70. Rudzka DA, Cameron JM, Olson MF. Reactive oxygen species and hydrogen peroxide generation in cell migration. Commun Integr Biol. 2015;8(5):e1074360. Epub 2015/12/30. doi: 10.1080/19420889.2015.1074360. PubMed PMID: 27066166; PMCID: PMC4802769.
71. Hu WG, Lu QP. Impact of oxidative stress on the cytoskeleton of pancreatic epithelial cells. Exp Ther Med. 2014;8(5):1438-42. Epub 2014/09/18. doi: 10.3892/etm.2014.1979. PubMed PMID: 25289036; PMCID: PMC4186494.
72. Sigaud S, Evelson P, González-Flecha B. H2O2-induced proliferation of primary alveolar epithelial cells is mediated by MAP kinases. Antioxid Redox Signal. 2005;7(1-2):6-13. doi: 10.1089/ars.2005.7.6. PubMed PMID: 15650391.
73. Nishio E, Watanabe Y. The involvement of reactive oxygen species and arachidonic acid in alpha 1-adrenoceptor-induced smooth muscle cell proliferation and migration. Br J Pharmacol. 1997;121(4):665-70. doi: 10.1038/sj.bjp.0701171. PubMed PMID: 9208132; PMCID: PMC1564732.
74. Wang Z, Castresana MR, Newman WH. Reactive oxygen and NF-kappaB in VEGF-induced migration of human vascular smooth muscle cells. Biochem Biophys Res Commun. 2001;285(3):669-74. doi: 10.1006/bbrc.2001.5232. PubMed PMID: 11453645.
75. Chubanov V, Ferioli S, Wisnowsky A, Simmons DG, Leitzinger C, Einer C, Jonas W, Shymkiv Y, Bartsch H, Braun A, Akdogan B, Mittermeier L, Sytik L, Torben F, Jurinovic V, van der Vorst EP, Weber C, Yildirim Ö, Sotlar K, Schürmann A, Zierler S, Zischka H, Ryazanov AG, Gudermann T. Epithelial magnesium transport by TRPM6 is essential for prenatal development and adult survival. Elife. 2016;5. Epub 2016/12/19. doi: 10.7554/eLife.20914. PubMed PMID: 27991852; PMCID: PMC5218537.
76. Parsons JT. Focal adhesion kinase: the first ten years. J Cell Sci. 2003;116(Pt 8):1409-16. doi: 10.1242/jcs.00373. PubMed PMID: 12640026.
77. Tani T, von Koskull H, Virtanen I. Focal adhesion kinase pp125FAK is associated with both intercellular junctions and matrix adhesion sites in vivo. Histochem Cell Biol. 1996;105(1):17-25. doi: 10.1007/BF01450874. PubMed PMID: 8824902.

78. Thomas JW, Ellis B, Boerner RJ, Knight WB, White GC, Schaller MD. SH2- and SH3-mediated interactions between focal adhesion kinase and Src. J Biol Chem. 1998;273(1):577-83. doi: 10.1074/jbc.273.1.577. PubMed PMID: 9417118.
79. Basuroy S, Dunagan M, Sheth P, Seth A, Rao RK. Hydrogen peroxide activates focal adhesion kinase and c-Src by a phosphatidylinositol 3 kinase-dependent mechanism and promotes cell migration in Caco-2 cell monolayers. Am J Physiol Gastrointest Liver Physiol. 2010;299(1):G186-95. Epub 2010/04/08. doi: 10.1152/ajpgi.00368.2009. PubMed PMID: 20378826; PMCID: PMC2904105.
61. Schroder K, Helmcke I, Palfi K, Krause KH, Busse R, Brandes RP. Nox1 mediates basic fibroblast growth factor-induced migration of vascular smooth muscle cells. Arterioscler Thromb Vasc Biol. 2007; 27:1736–43.